JOURNAL OF PETROLOGY | VOLUME 37 | NUMBER 6 | PAGES 1579–1600 | 1996

JEAN LOUIS VIGNERESSE[1]*, PIERRE BARBEY[2] AND MICHEL CUNEY[3]
[1]CREGU, BP 23, 54501 VANDOEUVRE, FRANCE; ALSO ECOLE NAT. SUP. GÉOLOGIE, NANCY, FRANCE
[2]LABO. PÉTROLOGIE, UNIVERSITÉ NANCY I, BP 239, 54506 VANDOEUVRE, FRANCE
[3]CREGU (ALSO GDR 77), CNRS-CREGU, BP 23, 54501 VANDOEUVRE, FRANCE

Rheological Transitions During Partial Melting and Crystallization with Application to Felsic Magma Segregation and Transfer

We consider the rheological behaviour of felsic magma in the zone of partial melting and during subsequent crystallization. We also introduce and combine concepts (mushy zone, percolation theory, granular flow, shear localization) derived from the non-geological literature and apply them to field observations on migmatites and granites. Segregation and transportation of felsic magmas is commonly observed in association with non-coaxial deformation, suggesting that gravity forces have limited influence during magma segregation. Solid to liquid and liquid to solid transitions are shown to be rheologically different, which infirms the concept of a unique rheological critical melt percentage for both transitions. Four stages are examined, which depend on the melt fraction present.

(1) A minimum of 8% melt by volume must first be produced to overcome the liquid percolation threshold (LPT) above which melt pockets can connect, thus allowing local magma displacement. Transport of the liquid phase is amplified by deformation toward dilatant sinks and is restricted to a very local scale. This corresponds to partially molten domains illustrated by incipient migmatites.

(2) When more melt (20–25%) is present, a melt escape threshold (MET) allows segregation and transport of the melt and part of the residual solid phase, over large distances. This corresponds to segregation and transfer of magma towards the upper crust.

(3) Segregation of magma also occurs during granite emplacement and crystallization. In a flowing magma containing few particles (≤20%), particles rotate independently within the flow, defining a fabric. As soon as sufficient crystals are formed, they interact to construct a rigid skeleton. Such a random loose packed framework involves ~55% solids and corresponds to the rigid percolation threshold (RPT). Above the RPT, clusters of particles can sustain stress, and the liquid fraction can still flow. The only remaining possibilities for rearranging particles are local shear zones, often within the intrusion rim, which, as a consequence, develops dilatancy. This stage of segregation during crystallization is totally different from that of magma segregation during incipient melting.

(4) Finally, the system becomes totally locked when random close packing is reached, at ~72–75% solidification; this is the particle locking threshold (PLT).

The introduction of four thresholds must be viewed in the context of a two-fold division of the cycle that generates igneous rocks, first involving a transition from solid to liquid (i.e. partial melting) and then a transition from liquid to solid (i.e. crystallization). Neither transition is simply the reverse of the other. In the case of melting, pockets of melt have to be connected to afford a path to escaping magma. This is a bond-percolation, in the sense of physical percolation theory. In the case of crystallization, randomly distributed solid particles mechanically interact, and contacts between them can propagate forces. Building a crystal framework is a site-percolation, for which the threshold is higher than that of bond-percolation. For each transition two thresholds are applicable. The present approach, which basically differs from that based on a unique critical melt fraction, expands and clarifies the idea of a first and a second percolation threshold. One threshold in each transition (LPT and RPT, respectively) corresponds to a percolation threshold in the sense of physical percolation theory. Its value is independent of external forces, but relies on the type and abundance of minerals forming the matrix within which melt connectivity is developing. The exact value of the second threshold (MET or

*Corresponding author. Telephone: 33 03 83 44 19 00.
Fax: 33 03 83 44 00 29. e-mail: jlv@cregu.cnrs-nancy.fr

PLT) will vary according to external forces, such as deformation and the particle shape.

KEY WORDS: *migmatites; partial melting; granites; magma segregation; magma solidification*

INTRODUCTION

The continental crust is a complex mixture of heterogeneous materials, but despite the differences in the mechanical and chemical properties of the various rocks, it can be considered on the whole to behave rheologically as a monophase. Under certain temperature and pressure conditions, however, this heterogeneous material may become polyphase as a consequence of partial melting. In this case, the rheological contrast between the molten and the solid phases leads to segregation processes that operate at all scales.

The present paper briefly describes the behaviour of partially molten systems and examines the segregation of liquid from solid phases as a function of the liquid percentage and the degree of deformation. We have attempted to compare field observations with theoretical or experimental studies (Van der Molen & Paterson, 1979; Hibbard & Watters, 1985; Wickham, 1987; Dell'Angelo & Tullis, 1988; Miller *et al.*, 1988; Hand & Dirks, 1992). Recent papers dealing with melt generation, segregation and crystallization include experimental studies, mostly on mafic and ultramafic rocks (Maaloe & Scheie, 1982; Marsh, 1989; Cooper, 1990; Waff & Faul, 1992; Hirth & Kohlstedt, 1995; Lejeune & Richet, 1995) but also on felsic rocks (Jurewicz & Watson, 1985; Johannes, 1988; Laporte, 1994). Numerical modelling has also resulted in important publications (e.g. McKenzie, 1984; Ribe, 1987). Recently, there has been renewed interest in this topic, based upon experimental (Rushmer, 1995; Laporte & Watson, 1995; Rutter & Neumann, 1995) and field observations (Brown *et al.*, 1995; John & Stunitz, 1997).

Because the processes (wetting of grain boundaries, segregation of a liquid phase, flow with suspended particles, shear localization) are not specific to magma flow, we have also considered theoretical studies of percolation and mechanical or chemical non-linear instabilities (Stauffer, 1985; Guyon *et al.*, 1990; Chvoj, 1993; Grinfeld, 1993). Studies from other fields which relate to similar phenomena encompass metallurgy, granular flows, non-Newtonian flows or liquid crystals and packing of particles (Wildenmuth & Williams, 1985; Carter, 1988; Campbell, 1990; Drake, 1990; Cazabat, 1991; Dlugogorski *et al.*, 1994; Rogers *et al.*, 1994). Previous studies have tried to model two-phase materials, using porous flow equations, slurry or debris flow models (McKenzie, 1984; Fowler, 1987; Bergantz, 1992; Worster, 1992; Major & Pierson, 1992; Coussot, 1994). Granular flow theory has been applied to sedimentation, flowing sands, or avalanches (Drake, 1990; Baxter & Behringer, 1991; Hutter & Koch, 1991). This represents a very large volume of literature, from which we have only cited a few key references, but investigated many more. Typically, the papers from the non-geological literature are very specialized and relate to very specific materials; therefore many must be read to obtain an overview of the ideas expressed. The other major problem comes from poorly illustrated papers, which makes the transferability of ideas, concepts and results to other fields difficult.

We attempt to clarify and rationalize these ideas to both the transition from solid to melt (i.e. partial melting) and the transition from melt to solid (i.e. crystallization). Reference is made mostly to felsic magma behaviour, but the application of these concepts to mafic or ultramafic magmas is briefly discussed. In subsequent discussions, we restrict the word 'melt' to crystal-free silicate liquids, whereas 'magma' refers to silicate melts which contain suspended crystals. We also systematically use the volume fraction of melt (F) or the volume fraction of first formed crystals (ϕ), and when explicitly needed, the degree of partial melting (F), which is a weight fraction.

RHEOLOGICAL TRANSITIONS IN MAGMAS

The generic cycle of felsic magmas starts from a source rock undergoing partial melting and ends with a fully crystallized magma. Migmatites are a good example of partially molten source rocks, whereas granitic intrusions display structures formed when magma stopped moving and crystallized.

The presence of a liquid phase in a partly molten rock severely modifies the bulk rheological properties of the whole rock. For instance, bulk viscosity varies by about six orders of magnitude from the solidus up to the liquidus. Consequently, the whole material behaves as a single phase at the very onset of melting, as two separate phases when melt segregates from the matrix, as a liquid with solid suspensions when magma is transported and ponds in the upper crust, or as a very viscous body at the end of its crystallization history. To model such large variations in the physical properties of the multiphase material, power law functions have been introduced,

mostly following the pioneering work of Einstein (1906). This led to the concept of a unique rheological critical melt percentage (RCMP) for the transition of a liquid to a solid (Arzi, 1978), later applied to a solid undergoing partial melting (Van der Molen & Paterson, 1979). However, because of the sudden transition from a viscous body to a locked solid, we suggest a reformulation through percolation theory (Stauffer, 1985).

Percolation theory has previously been applied to partially molten materials (Blanchard, 1978; Nicolas, 1986; Nakano & Fujii, 1989). A refinement has recently been proposed with the introduction of two critical values for the melt percentage. A first percolation threshold occurs when melt films at grain boundaries are connected and a second one exists for melt escape (Vigneresse *et al.*, 1991; Sawyer, 1994). Because they operate under different conditions during partial melting and crystallization, we separately examine both transitions so as to better constrain the factors controlling magma rheology. During a melting and crystallization cycle (Fig. 1a, 1b), we define four thresholds which depend, in gross terms, on the melt fraction present, and control the movement or segregation of the liquid phase.

(1) A minimum of 8% liquid by volume must first be produced to overcome the liquid percolation threshold (LPT) above which a continuous melt film along grain boundaries connects melt pockets. Melt transport is mainly restricted to a local scale and may be amplified by deformation toward dilatant sinks (Fig. 1a).

(2) When more melt (20–25%) is present, a melt escape threshold (MET) allows segregation and transport of the magma, and to a certain extent, the residual solid phase, over large distances. This corresponds to segregation and transfer of magma towards the upper crust (Fig. 1a).

(3) Segregation of magma also occurs during granite emplacement and crystallization. In a flowing magma containing few particles ($\leqslant$20%), particles rotate independently in the flow, defining a fabric (Fig. 1b). As soon as sufficient crystals are formed, they interact to construct a rigid skeleton. Such a random loose packed framework involves about 55% solids and corresponds to the rigid percolation threshold (RPT). Above the RPT, clusters of particles can sustain stress, and the liquid fraction can still flow. The only remaining possibilities for rearranging particles are local shear zones developing dilatancy, preferentially within the intrusion rim. This stage of segregation during crystallization is totally different from that of magma segregation during incipient melting.

(4) Finally (Fig. 1b), the system becomes totally locked when random close packing is reached, at ~72–75% solidification; this is the particle locking threshold (PLT).

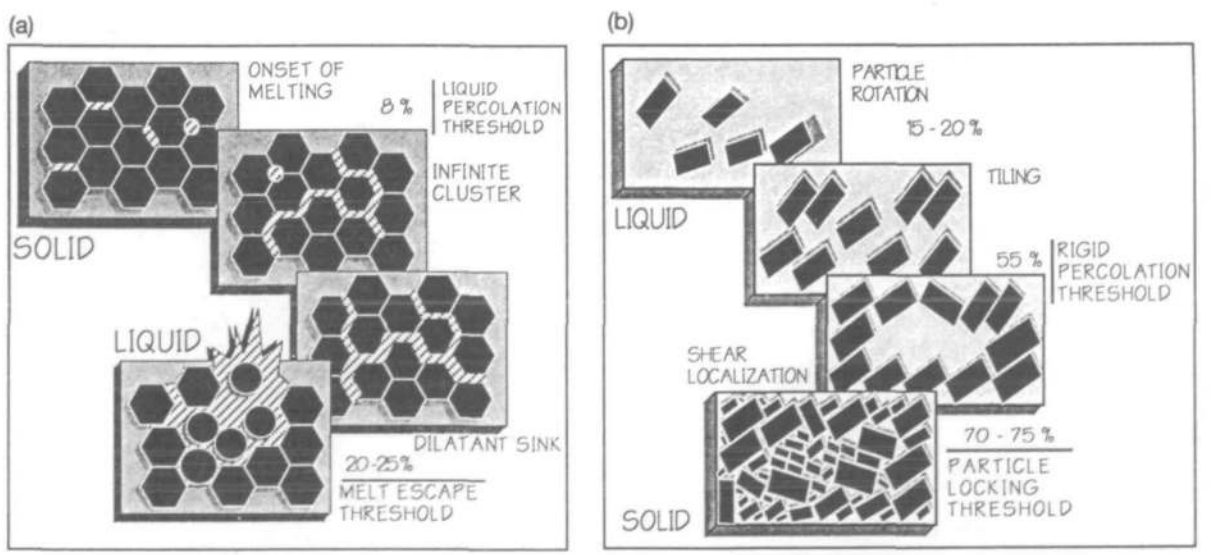

Fig. 1. (a) Schematic rheological transitions in partially molten systems. The transition from solid to liquid is indicated with the onset of melting and grain boundary wetting, up to connection of an infinite cluster, thus defining the liquid percolation threshold (LPT). With continuing melting, melt can move up to escape its matrix at the melt escape threshold (MET). (b) The transition from liquid to solid is not the converse, or the dual, of the former transition. At low particle percentage, particles freely rotate, and tile up to the rigid percolation threshold (RPT), in which the rigid but weak framework can sustain stresses. At higher particle percentage, dilatancy and shear localization occur, up to a particle locking threshold (PLT).

Einstein–Roscoe equations

Most papers referring to partially molten material behaviour quote Arzi (1978) and Van der Molen & Paterson (1979): the viscosity calculation proposed by Arzi refers either to the experiments of Einstein (1906) or to those of Roscoe (1952). In the proposed relationship, the relative viscosity (η) of a suspension of rigid particles is given, in its correct form [see Roscoe (1952)], by

$$\eta = (1 + a\phi)^n \quad (1)$$

where ϕ is the particle concentration, and a and n are experimentally determined coefficients. In Roscoe's original paper, $a = -1{\cdot}35$ and $n = -2{\cdot}5$. Because this equation has been widely, perhaps too widely, used in subsequent papers (Wickham, 1987; Miller *et al.*, 1988), we briefly discuss its merits.

General equations of transport for polyphase materials have been developed extensively in a literature ranging from mathematics to applied technology [see Jinescu (1974) for a review containing 133 references]. The simplest approach, valid for dilute suspensions, uses a linear development:

$$\eta = (1 + a\phi + b\phi^2 + \ldots) \quad (2)$$

For very dilute suspensions, Batchelor (1983), amongst others, gave an adequate solution with $a = 1{\cdot}5$, whereas $a = 1{\cdot}3 \pm 0{\cdot}2$ has been suggested for denser suspensions (Batchelor, 1976). Taking into account particle interactions at larger distances extends the formula to the second order (Cox & Brenner, 1971). Adopting a more theoretical point of view, Hori & Yonezawa (1975) used perturbation theory to describe the change in the transport properties of an average medium of viscosity $<\eta>$ owing to a perturbed value, the average of the perturbation being $<\eta'>$. They also presented linear relationships, but used the generalization of Kröner (1978), which develops the complete series in a function

$$\eta = 1 + \sum_{n=2}^{\infty} \left(-\frac{1}{3}\right)^{n-1} \frac{<\eta'^n>}{<\eta>^{n-1}} \cdot <\ldots> \quad (3)$$

Though the development is not straightforward, this series can be transformed into a more convenient formula (Kröner, 1978):

$$\eta = <\eta A> \; <A>^{-1} \quad \text{with } A = (I + G\partial\eta)^{-1} \quad (4)$$

in which I is the identity matrix, G is a Green function which operates on the pertubation $\partial\eta$ and the symbol $<.>$ indicates averaged values. This reformulates the Einstein–Roscoe law in a more compact form and bears similar physical meaning, as

$$\eta = (1 + a_1\phi + a_2\phi^2 + \ldots) \equiv 1/(1 - a\phi)^n \quad (5)$$

in which a corresponds to the inverse of the minimum porosity left during packing.

Whatever the formula (1)–(4) used, the coefficients of this kind of linear development have been experimentally determined for a variety of solid particles, and hence with very different geometrical properties [see, e.g. the review by Jinescu (1974)]. In addition, other non-linear terms have been added to fit the experiments. Consequently, experimentally determined curves spread when plotted on the same diagram (Fig. 2), and the values of the relative viscosity vary by two orders of magnitude for a fixed melt percentage (50%). Though the bulk trend is similar, and thus validates the Einstein–Roscoe equations, the curves differ because of the final packing value of the concentrated solution. The progressive curving toward a steeper increase of the relative viscosity reflects the increasing degree of packing.

Because of this constraint, all preceding laws are, in essence, limited to dilute or to moderate concentrations of particles. This has recently been experimentally verified for a melt with pyrope composition, containing up to 40% by volume solid Al-enstatite spheres (Lejeune & Richet, 1995). However, the multiplicity of equations and the spread of experimentally determined data are not in favour of such a formulation.

Furthermore, this type of equation, determined for a suspension of particles, is not directly relevant to the problem of a solid undergoing melting. The rheological critical melt percentage (RCMP) of 25–30% (Arzi, 1978) corresponds to the transition from

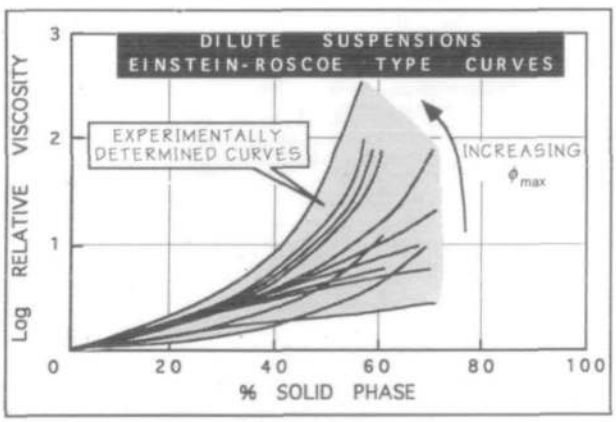

Fig. 2. Experimental curves of relative viscosity variation, based on Jinescu (1974), showing the range of the results obtained using Einstein–Roscoe derived equations, or virial expansion of the viscosity equations. Because of the strong dependence of the equations on particle shape and packing, the curves shift to higher viscosities according to the increase in maximum packing (ϕ_{max}). Two orders of magnitude in variation of the relative viscosity can exist for a concentration of 50% of solids.

a loose packing to a coherent medium. In no case is its value a function of deformation. The only influence deformation can have on the value of the RCMP is to increase the maximum packing value, thus reducing the minimum porosity left within the matrix, and consequently to decrease the coefficient a in equation (1).

Percolation and transition thresholds

Two types of percolation (Fig. 3) are identified in theoretical physics (Stauffer, 1985). One, called bond-percolation, is achieved when connection is realized in a network (e.g. wetting of grain boundaries by liquid during incipient melting); the other, called site-percolation, occurs when randomly distributed spots achieve connectivity by juxtaposition (Fig. 3). When such a connection is realized, it defines an infinite cluster. The percentage to which infinite cluster occurs determines the percolation threshold (p_c). This threshold is in essence dependent on the network on which it is realized. However, the power law describing the probability of occupancy near the threshold presents a coefficient independent of the nature of the network. It thus reflects a more general law, valid whatever the nature of the model. Because of the easier connection by bonds, the bond-percolation threshold is lower than the site-percolation threshold. The transition from solid to liquid represents a bond-percolation, whereas crystallization is considered as a site-percolation.

The liquid percolation threshold (LPT) is adequate for describing a solid undergoing melting. It corresponds to the amount of melt which can wet grain boundaries to form a continuous film throughout the material. Our suggested value for the LPT, at ~8% for felsic melts, is consistent with values inferred from experiments conducted at high confining pressures and temperatures (<10% for felsic rocks; Rushmer, 1995; Rutter & Neumann, 1995), and from experimental and theoretical studies on percolation theory (Stauffer, 1985). The bond-percolation threshold (p_c) computed for 3D lattices is 0·249 for a simple cubic lattice, but decreases to 0·119 for a face-centred cubic lattice. For Bethe lattices, defined by a repeated infinite branching process with coordination number Z, the percolation threshold can be estimated as $p_c = 1/(Z-1)$, which leads to small threshold values. Numerical simulations using equal-sized spheres indicate that Z, usually four for random loose packing, increases to six for a random packing of spheres, and even to 12 for a dense packing (Guyon *et al.*, 1990; Nolan & Kavanagh, 1992). It also increases with polydispersity of solutions, i.e. when spheres with different radius are mixed together. We suggest a value of 8% for dense packing, equivalent to a coordination number $Z = 12$. This value also fits observations in partly molten gneisses. Experiments on quasi-monomineralic mafic material indicate that the LPT starts at a very few percent (Nakano & Fujii, 1989). Values of 5% and down to 1% were derived from experiments performed respectively on ultramafic material (Hirth & Kohlstedt, 1995) and olivine–basalt systems (Daines & Richter, 1988). However, for a larger number of uniformly distributed phases, as observed in felsic rocks, the threshold is nearer to that of a 3D random lattice, that is, ~8%. Whatever the threshold values, the LPT should not be confused with the RCMP, which had been coined for an increasing proportion of solid phase in a suspension.

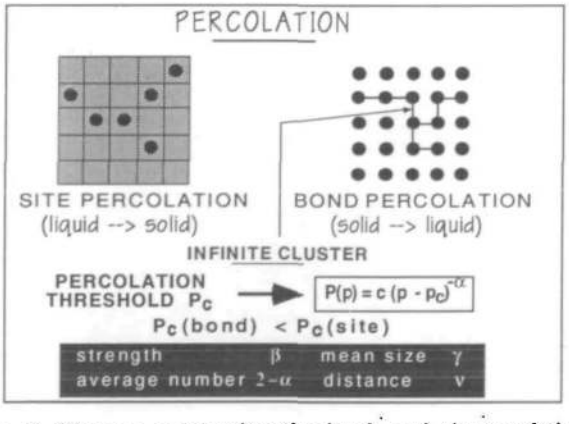

Fig. 3. Diagram representing the bond- and site-percolation processes which lead to the formation of an infinite cluster throughout the system. Near that transition, or percolation threshold (p_c), the probability of site occupation is governed by a power law, the coefficient of which (α) is independent of the geometry of the system. The specific coefficients of the power laws related to the geometry of clusters (mean size, distance or correlation length, average number and strength; see text) are also indicated.

The rigid percolation threshold (RPT) that occurs during crystallization is different from the LPT. Minerals, when crystallizing, grow up to form grain-to-grain contacts and thus define a site-percolation, as the resulting semi-rigid framework can transmit stress (Fig. 3). The site-percolation threshold is higher than the bond-percolation threshold. Indeed, when two sites are connected by an open bond, it can be viewed as a cluster of size two (i.e. two sites are connected) or of size one (i.e. the bond between two sites). The threshold value is, thus, reduced by about a factor of two in the case of a 3D regular lattice (Stauffer, 1985). According to our estimates of random loose packing, the percentage of solid present at the RPT is high (55%). This implies that 45% of melt is still present, which is also high compared with the amount of melt at the LPT (8%).

The importance of the percolation threshold is relevant to the behaviour of some scaling equations near the transition (Fig. 3). They are power dependent in the form $(p-p_c)^{\alpha}$, where p is the probability of site, or bond, occupancy near the percolation threshold p_c, and α is a constant independent of the lattice (Stauffer, 1985). Such power laws can be computed for the mean size of finite cluster (i.e. the length of connected particles), the correlation length (the distance between clusters), and the average number (number of particles in one cluster) or the strength of the clusters (similar to an inertia momentum of clusters). In each case, an invariant coefficient defines the power law, independent of the network (Fig. 3). Such coefficients could be used to test the validity of the percolation theory, provided a convenient procedure is designed for measuring such variables during melting or magma crystallization.

Granular flow and local dilatancy

As the number of particles increases, they are less free to rotate independently, contacts between them become dominant and the material enters the domain of granular flow (Jenkins & Savage, 1983; Campbell, 1990; Drake, 1990). This theory has been analysed in 2D on discs and in 3D on spheres, but has also been modelled using orientable particles (Savage & Sayed, 1984; Baxter & Behringer, 1991; Dlugogorski *et al.*, 1994). Certainly, fast granular flows (e.g. avalanches) exchange kinetic energy at a higher rate than solid particles during collision in a magma flow. However, the concept of granular flow basically concerns concentrated suspensions. The large number of particle interactions provides a fast transfer of momentum, whatever the quantity of momentum exchanged. During collisional contacts, momentum and energy are exchanged between particles more or less proportionally to the flow velocity (Babic *et al.*, 1990). This exchange is more effective in transferring momentum parallel to the shear surface, thus developing shear stress (Savage & Sayed, 1984). At low solid density, the stress depends on the solid density, yielding Bagnold effects (Komar, 1976), whereas the stress departs from a square shear rate at higher density.

In the case of discs with an interstitial liquid phase, a rapid granular flow is observed for solid percentage (ϕ) up to 55%. In the case of 3D modelling, at the onset of granular flow, particle distribution defines a dense state, close to random loose packing, that is, ~51–55%. Subsequently, particles aggregate (Babic, 1993) and a transition in the distribution of contacts occurs, from disc pairs in contact, which make an angle of 60° to the shear flow, to quadruplets with contacts at 60° and 120° to the shear flow. This occurs at 0·8 of the maximum packing value, that is, for ϕ of ~66% (Babic, 1993). During the transitional stage, clusters of particles form, which remain stable, whereas all deformation is accommodated at the border of the cluster. This represents a near continuum of touching particles but liquid is still present (~45%). Because of the rigid state of the crystals, the resulting matrix can support a load. The suspension can accommodate hydrostatic forces as well as shear stress transmitted through the weak frame of rigid crystals (no internal shear of particles). It defines an infinite cluster in the sense of percolation theory. The concept of a rigid percolation threshold (RPT) has been coined for this stage (De Gennes, 1979; Garboczy & Thorpe, 1985).

As packing increases, shear displacements result in an outward acting hydrostatic stress at the system boundary. The random loose packing thus corresponds to the onset of Reynold dilatancy (Onoda & Liniger, 1990). This effect is well known in sandy beaches, where foot compression on the water-impregnated sand induces a movement of the particles, which first results in an increase of the void density, drying the sand at the surface, and then the achievement of a denser packing (Fig. 4). It is a function of the dilation angle (α) which characterizes the particle displacement. The resistance to shear is proportional to the hydrodynamic stress and increases with packing. As a result, the friction angle increases, inducing shear thickening (Barnes, 1989; Bashir & Goddard, 1991). As clusters form, the movement of particles themselves is stopped, and

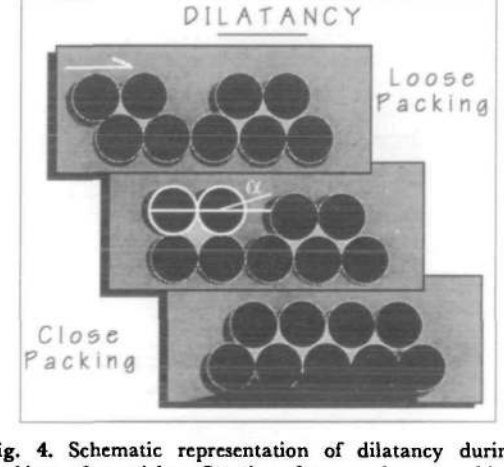

Fig. 4. Schematic representation of dilatancy during denser packing of particles. Starting from a loose packing (upper diagram), particles (in the middle diagram) have to pass over the surrounding ones to reach higher packing (lower diagram). The angle α corresponds to the dilation angle, determined by the geometry (with increase of space) a particle has to follow to attain higher packing.

strains must concentrate in zones where fluid remains continuous and can accommodate deformation. This is similar to strain localization in deforming plastic material at low temperature (Harren *et al.*, 1988; Schaeffer, 1992). Accommodating stress by strain localization at the border of the system is the ultimate response of a nearly locked system, which can only accommodate strain locally, but no longer on a large scale. It corresponds to local shear zones observed in granitic and mafic intrusions (Blanchard *et al.*, 1979; Brun *et al.*, 1990; Nicolas, 1992; Pons *et al.*, 1995). However, this stage is not the stage of highest packing yielding absolute rigidity, which is reached at the close packing value ($\phi = 72$–75%).

MELTING AND SEGREGATION IN MIGMATITIC COMPLEXES

Common migmatites are made up of leucocratic and melanocratic layers, respectively referred to as leucosome and melanosome, associated with more or less modified metamorphic rocks called mesosome and unfused material (restites). In some cases, the melting of feldspathic quartzites can lead to the formation of leucocratic restites (Cuney & Barbey, 1981). As we are dealing with melt–solid relationships, metamorphic differentiation has not been considered here. Numerous mineralogical and structural criteria show that leucosomes are crystallized melts: (1) near-minimum melt composition (e.g. Johannes, 1988); (2) geochemical mass balance between leucosome, melanosome and palaeosome; (3) microtexture and composition of minerals (e.g. Weber *et al.*, 1985; McLellan, 1988); (4) spatial relationships; (5) melt accumulation near a non-permeable layer; (6) incipient diapirism or hydraulic fracturing (Burg & Vanderhaeghe, 1993). Therefore, migmatites can be viewed as a two-phase mixture with strongly contrasting rheological properties (Fig. 1a). Depending on the distribution and relative proportions of the two phases, their bulk rheological properties may vary drastically.

Melt–solid proportions

Depending on the original source composition, the amount of liquid compared with solids may vary considerably over short distances, reaching very high values within leucosomes (>80%), whereas it can still be very low in mesosome or even nil in restites. A distinction should be made between F, the degree of melting, or the fraction of melt formed by fusion of a particular rock volume, which can be equated approximately to the leucosome/(leucosome + melanosome) ratio under closed-system conditions, and P, the bulk melt percentage, that is, the ratio of the mobile fraction (leucosome) to the whole volume of rock (leucosome + melanosome + unmelted lithologies).

In most cases, the leucosome is not necessarily a liquid, but can include a more or less abundant fraction of restitic minerals (calcic plagioclase, quartz and femic minerals). In addition, some liquid may exist between melanosome grains, but cannot be mobilized, except under shearing. Consequently, P may be significantly lower than F, as exemplified by the stromatic migmatites (Johannes, 1988). Assuming a mesosome/leucosome ratio of 5:1, with incomplete melting and segregation, so that $F = 0{\cdot}8$ in the leucosome and $F = 0{\cdot}1$ in the mesosome, leads to a total amount of mobile material (P) of ~22% of the whole rock volume.

In fact, the concept of degree of melting (F) mainly relates to mineral and melt chemistry, whereas P relates to rheology. The two thresholds we propose can respectively be related to melt connectivity, which basically relies on F (LPT), and then to melt instability, which depends on both F and P (MET).

Thresholds

Under incipient melting conditions, melt distribution along grain boundaries is controlled by phase assemblages (e.g. Mehnert & Büsch, 1982) and the dihedral angles between the liquid and adjacent crystals (Jurewicz & Watson, 1985), because of textural equilibration. However, this is hardly discernible in natural examples. Partly molten gneisses show ~8% of visible melt before a connection is realized between melt pockets (Fig. 5a).

Once connectivity is achieved, corresponding to ~8% of melt in volume, the liquid percolation threshold (LPT) is reached. Segregation occurs, as shown by the centimetre- to decimetre-scale leucosome lenses surrounded by millimetre-thick restitic rims of refractory minerals found in migmatites. Melt segregation is considered to be controlled by diffusion processes at the very onset of melting, then by buoyancy forces, though non-coaxial deformation becomes rapidly dominant. It may be driven by fluid phases (Olsen, 1985; Maaloe, 1992; Fourcade *et al.*, 1992). Nevertheless, the melt cannot be transported far from its source zone, and the system still behaves as a closed system. This is shown by the close chemical similarity of some partially melted metapelitic gneisses to their sedimentary protolith (e.g. Barbey *et al.*, 1990). This stage extends roughly from the beginning of melting around 620–650°C up to 750°C

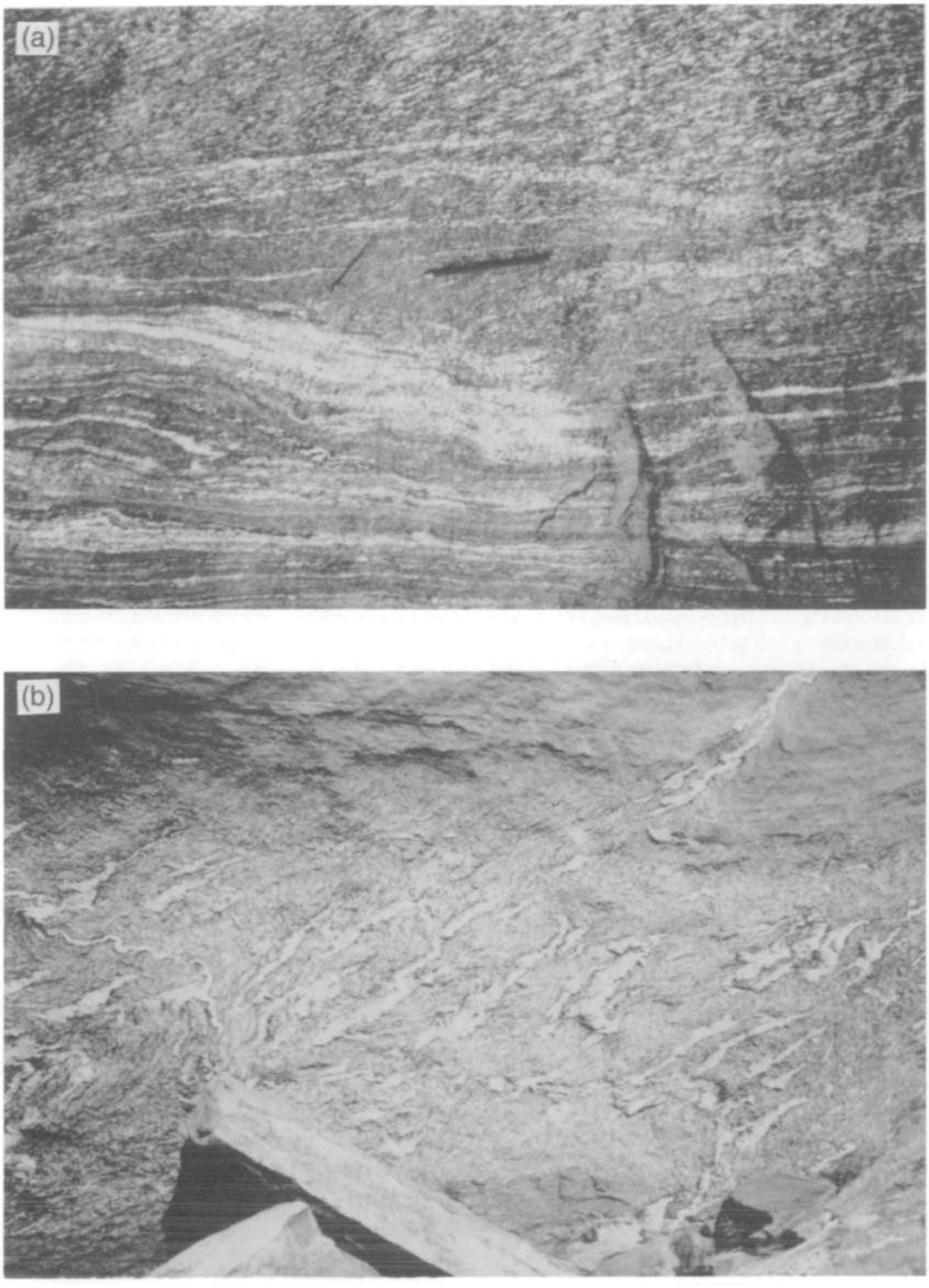

Fig. 5. (a) Unconnected melt pockets in a partly molten gneiss from Paraiba (NE Brazil). (b) Segregation of melt in migmatites, from Currais Novos migmatites (NE Brazil). This clearly shows the trend of leucosome veins at a high angle to the NW–SE orientation of σ_1 which induces a dextral, top to the east, shear to the outcrop.

before dehydration melting begins (see Clemens & Vielzeuf, 1987; Vielzeuf & Holloway, 1988).

The melt segregation rate remains very low and very little liquid is extracted from its matrix under static conditions, i.e. without deviatoric stresses. Compaction alone (McKenzie, 1984; Wickham, 1987) is not very efficient because the creep rate of the matrix is large compared with the flow rate of the melt (Maaloe & Scheie, 1982; Ribe, 1987). Even in case of melts of very low viscosity (10^4 Pa s), the compaction length, which hardly reaches hundreds of metres, is not sufficient to allow a large-scale segregation of melt (Petford, 1993). Non-coaxial forces must be added to squeeze out the melt from its matrix. At the microscopic scale, the melt distribution varies according to the degree of deformation (Dell'Angelo & Tullis, 1988; Laporte & Watson; 1995; Jin *et al.*, 1995). Melt spreads along grain boundaries when the sample is subjected to low stress creep or when grain boundaries are already mostly aligned (Hirth & Kohlstedt, 1995). However, at the mesoscopic scale, observations on natural samples and experimental results (McLellan, 1988; Cooper, 1990; Hand & Dirks, 1992) indicate that the melt segregates towards the region of lower stress, usually oriented at a high angle to σ_1 or parallel to σ_3 toward the sector of extensional stretching (Fig. 5b). Deformation-assisted pumping of partial melts towards dilatant sinks is favoured. Structures related to this process are extensively illustrated in textbooks on migmatites and related publications (e.g. McLellan, 1988; Sawyer, 1991; Macaudière *et al.*, 1992). These examples emphasize the importance of non-coaxial deformation, which is predominant in migmatites and in molten gneisses, versus buoyancy or gravity driven forces. Nevertheless, although magma can be segregated over short distances, it still remains near its source and large-scale transport is a subsequent stage of the process. The balance between magma pressure and σ_3 controls the escape of the melt.

If melting rate is higher than segregation rate, the melt escape threshold (MET) is reached at $P = 20$–25%, and melt transfer over large distances becomes possible (Sawyer, 1994). This condition is likely to be satisfied when dehydration melting conditions are reached, i.e. above 800°C. These reactions abruptly increase melt fraction (Vielzeuf & Holloway, 1988; Patiño Douce & Beard, 1995), which in turn increases the bulk melt percentage P. Cohesion can no longer be sustained and shear localization develops which segregates and expels the melt from its intergranular sites. Because the whole system is closed and still behaves coherently under deformation, the increase of pressure owing to the expansion volume of the melt ($\sim 10\%$) can lead to the development of a conjugate fractures system (Davidson *et al.*, 1994). Such a value of $P = 20\%$ is also the threshold value that marks a change from a closed system segregation to an open system escape of melt (Petford, 1993). The movement of melt is then accelerated, and switches from a diffusion mode to an advection mode. Mechanical segregation operates at a metre scale, yielding cauliflower structures, vein clusters and asymmetric apophyses that may be used as way-up criteria (Burg & Vanderhaeghe, 1993).

This transition is clearly visible in migmatite terrains, as shown in the following examples. The first example is the Saint Malo migmatites, shown to have formed from high degrees of melting (F) up to 70–80% (Weber *et al.*, 1985). The Saint Malo migmatitic dome grades from metatexites in the periphery to diatextites and anatectic granites in the core. Intense shearing recorded by strong structural criteria (quartz *c*-axes girdles, non-coaxial shear bands) is observed on both sides of the migmatitic massif (Brun & Martin, 1978). Opposite senses of shear on each side of the massif reflect strong movement of its interior part relative to the surroundings, suggesting 'en-masse' ascent of the whole partially melted body.

In a second example, the Yaoundé migmatites (Barbey *et al.*, 1990), two types of melt are observed to coexist:

(1) *in situ* partial melts produced by a low degree of melting ($F < 0{\cdot}15$); these occur as lenses conformable with the schistosity or collected in shear zones, and record regional deformation implying that the whole migmatitic body, though it incorporates a non-negligible melt fraction, still behaves as a solid body; and

(2) material formed from a high degree of melting ($F \geqslant 0{\cdot}50$) and injected as concordant or cross-cutting decimetre-thick veins.

Lastly, in the Velay anatectic dome, two phases of migmatization have been recognized, which probably represent one of the most remarkable examples of a transition from low ($<$MET) to high ($>$MET) P values related to changing temperature conditions (Montel *et al.*, 1992). The first stage develops under moderate temperature (biotite stable; $T < 750$°C) and leads to migmatites with a low bulk melt proportion. Leucosomes occur as lenses conformable with the schistosity, but are also redistributed in areas of lower strain such as fold hinges, conjugate shear zones, veins, and extensional zones between boudins (Macaudière *et al.*, 1992). Nevertheless, the whole massif behaves as a solid

entity and records the regional deformation (large-scale recumbent folds). The second stage developed through dehydration-melting (cordierite stable; $T \geqslant 800°C$) and led to high melt percentages. Cohesion is lost, the former tectonic structures are erased and the whole massif behaves as a magma. This stage corresponds to the emplacement of the Velay dome (Montel *et al.*, 1992).

Relation to deformation

Migmatization is intimately related to deformation. Most regional studies have described migmatitic outcrops as domal structures (Brun & Martin, 1978; Sawyer & Robin, 1986; Nzenti *et al.*, 1988; Jones & Brown, 1990; Montel *et al.*, 1992). This is shown, for instance, by the concentric zonation of metamorphic isograds, with very steep thermal gradients (~160–200°C/km) and symmetric ductile deformation observed around the massifs.

Comparison of synthetic P–T–t paths of various migmatites (Fig. 6) with deformation patterns suggests that there is some systematics in the succession of deformation styles. This can be seen in most migmatitic massifs: Saint Malo, Yaoundé, Velay dome, Port-Navalo, Quetico Metasedimentary Belt, Himalaya (Brun & Martin, 1978; Weber *et al.*, 1985; Sawyer & Robin, 1986; Weber & Barbey, 1986; Sawyer & Barnes, 1988; Nzenti *et al.*, 1988; Jones & Brown, 1990; Barbey *et al.*, 1990; Brouand *et al.*, 1990; Montel *et al.*, 1992; Barbey *et al.*, 1995). A continuum between three styles of deformation can be observed (Fig. 6). These can be considered as reflecting a change in the rheology with time when the LPT and MET are crossed. One (D_1) corresponds to a regional deformation event associated with metamorphic recrystallization. Mainly developed under subsolidus conditions, it ends with incipient melting conditions. Structures show evidence of melt migration but only over short distances, and the whole unit behaves as a solid body and records the regional deformation. The subsequent phase (D_2) is synchronous with the peak temperature and extensive melting. It also shows abundant evidence of non-coaxial deformation and corresponds to the destruction and disappearance of the former structures leading to diatexites and granites. This phase corresponds to the global uplift of the migmatitic unit leading to the individualization of anatectic domes. The third (D_3) occurs after the initial thermal perturbation, under decreasing temperatures, from near-solidus to subsolidus low-temperature conditions. It develops local shear zones filled with leucosomes, faults associated with medium-temperature mylonites, and low-temperature veins and tension gashes filled with quartz.

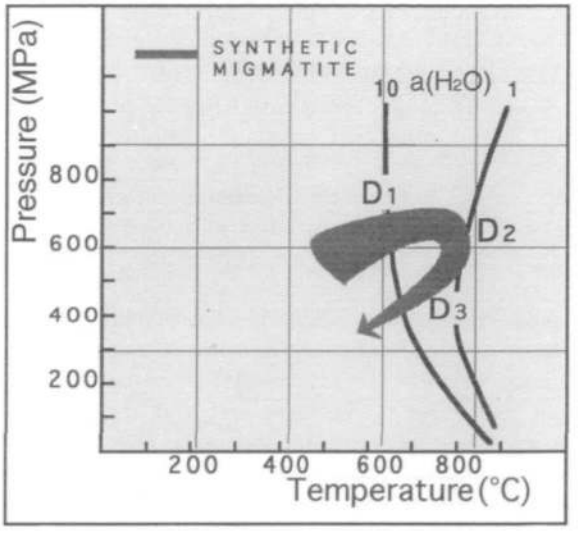

Fig. 6. P–T diagrams for various migmatites referenced in the literature and associated deformation. A synthetic P–T path (in grey) has been inferred from this data set with the usual three phases of deformation. The first stage of deformation (D_1) occurs during the increase in temperature. It is followed by a second phase (D_2) when melting is generalized, usually by dehydration reactions, to the whole body. The late stage of deformation (D_3) occurs after the decrease in pressure (upwelling of the migmatitic body). Also shown are the solidus curves of an average granitic magma for water activity (a_{H_2O}) of 1 and 10.

EMPLACEMENT AND CRYSTALLIZATION OF GRANITIC MAGMAS

Transport of magma and fabric acquisition

Above the melt escape threshold, and because liquids are buoyantly unstable, they are usually transported upwards. This constitutes the principal mass transfer mechanism in a continental crust undergoing partial melting, and can lead to granitic plutons emplaced into the upper crust. However, gravity forces are less effective in segregating magma than non-coaxial forces.

The transport of partly molten material is far from being homogeneous. Mechanical interactions between solid particles during magma flow induce a grain dispersive pressure proportional to the rate of shear. A transverse velocity and momentum are generated, which are perpendicular to the flow direction. This mechanism induces the well-known Bagnold effect (Bagnold, 1954; Komar, 1976; Blanchard *et al.*, 1979). It should not be confused with the Magnus effect, which results from a differential

translatory motion of the fluid which induces particle rotation (Barrière, 1976). This effect, or wall effect, decimetric in scale, is restricted to small conduits.

The anisotropic distribution of velocity owing to particle interaction is quickly attenuated in wider channels, in which the flow becomes mostly uniform. In a larger volume such as that leading to granitic intrusions, the flow is laminar and gives rise to magmatic structures. At low strains, depending on the volume percentage (ϕ) of crystals, the magma behaves as a viscous body ($\phi \ll 55\%$), a framed viscous body ($55\% < \phi < 75\%$) or a rigid entity ($\phi > 75\%$). The transition from viscous to rigid behaviour varies according to the increasing strain rate, as noted by Arzi (1978), Van der Molen & Paterson (1979), Dell'Angelo & Tullis (1988) and Miller *et al.* (1988). These workers have defined a rheological critical melt percentage (RCMP of $\sim 28\%$ of melt) which corresponds to the beginning of plastic deformation within matrix crystals. For example, in dense crystal frameworks, quartz aggregates typically show intracrystalline deformation features (Blumenfeld & Bouchez, 1988; Gapais, 1989).

When the solid particles are few, they rotate because of the shear flow and induce a fabric in the rocks. This has now been analysed (Ogawa *et al.*, 1973), and numerically or experimentally reproduced (Fernandez *et al.*, 1983; Ildefonse *et al.*, 1992). In the prevailing laminar flow regime, the flat and elongated crystals develop a monoclinic fabric (Fernandez, 1987) which can be determined through the usual structural methods (Blumenfeld & Bouchez, 1988; Gleizes *et al.*, 1993). Foliation planes can be easily observed as the planar fabric developed by the average orientation of restitic enclaves (Fig. 7a) or of the first formed crystals (Fig. 7b). The associated lineation is determined by the average elongation of the crystals, or by the zone axis of their large face orientation. The sense of flow can then be estimated, provided shear criteria can be recognized (Gapais & Barbarin, 1986; Blumenfeld & Bouchez, 1988).

Coherent structural patterns are observed in granitic plutons (Guineberteau *et al.*, 1987; Gleizes *et al.*, 1993), but also in mafic intrusions and ophiolites (Nicolas, 1992; Ernst & Baragar, 1992). In granites, the flow pattern (e.g. in Saint Sylvestre—see Fig. 9, below) is organized at the scale of successive magma pulses (Mollier & Bouchez, 1982; Gleizes *et al.*, 1993). A coherent pattern may diverge from the apex of the root zones. This implies that the flow is laminar, without large disturbances, with the exception of those regions at the limits of the massif and at the contact with previous magma pulses. Fabrics are acquired close to the root zone and do not evolve significantly subsequently while magma migrates toward its present location within the massif.

A coherent fabric pattern is observed in many granitic intrusions to be grossly divergent from the root zones. These are easily determined by steep dipping lineations and a deeper floor inferred from gravity data inversion (Vigneresse, 1995). However, no return descending flow pattern has yet been recognized in granitic plutons though fabrics are acquired very early in the magma history at ~ 10–20% crystallization. In consequence, convective overturn cannot be traced within granitic plutons. This limits the viscosity of the magma. If a pluton is ~ 5 km thick, its bulk viscosity will be $\sim 10^{10}$ Pa s at the time of its emplacement.

At higher percentage of particles, interactions between particles become predominant. Particles cannot freely rotate any more and tile against each other (Blumenfeld, 1983; Blumenfeld & Bouchez, 1988)

Late segregation of magma

Following its emplacement, the intrusive body crystallizes and may still deform according to the regional stress field (Fig. 1b). As soon as particles aggregate, they form a weak frame of rigid crystals which can sustain forces. Such random loose packing defines the rigid percolation threshold (RPT). The crystalline framework precludes large-scale movement of the whole magmatic body, and the movement of the residual melt is inhibited. Finally, at the particle locking threshold (PLT), or random close packing, no more magma can escape the system without deformation, and full crystallization ends the process. Between these stages, deformation is plastic, though fractures may occur, depending on the temperature and on whether feldspar or quartz is the dominant mineral (Fig. 8b). The process is not the reverse of the transition to melting, because, as magma crystallizes, its viscosity increases, but the residual melt becomes either more mobile or more viscous, depending on its composition and fluid phase (Holtz & Johannes, 1994).

Before being totally locked, the system evolves by reacting to the regional stress field and segregating the residual melt (John & Stunitz, 1997). Deformation develops which destabilizes the weakly rigid framework formed by the crystals, inducing non-coaxial structures and removal of the remaining melt fraction enriched in incompatible elements. In granitic plutons, such structures are observed at all scales from metric (Fig. 8a) to kilometric. They have been remarkably illustrated in the Birimian Nigerian

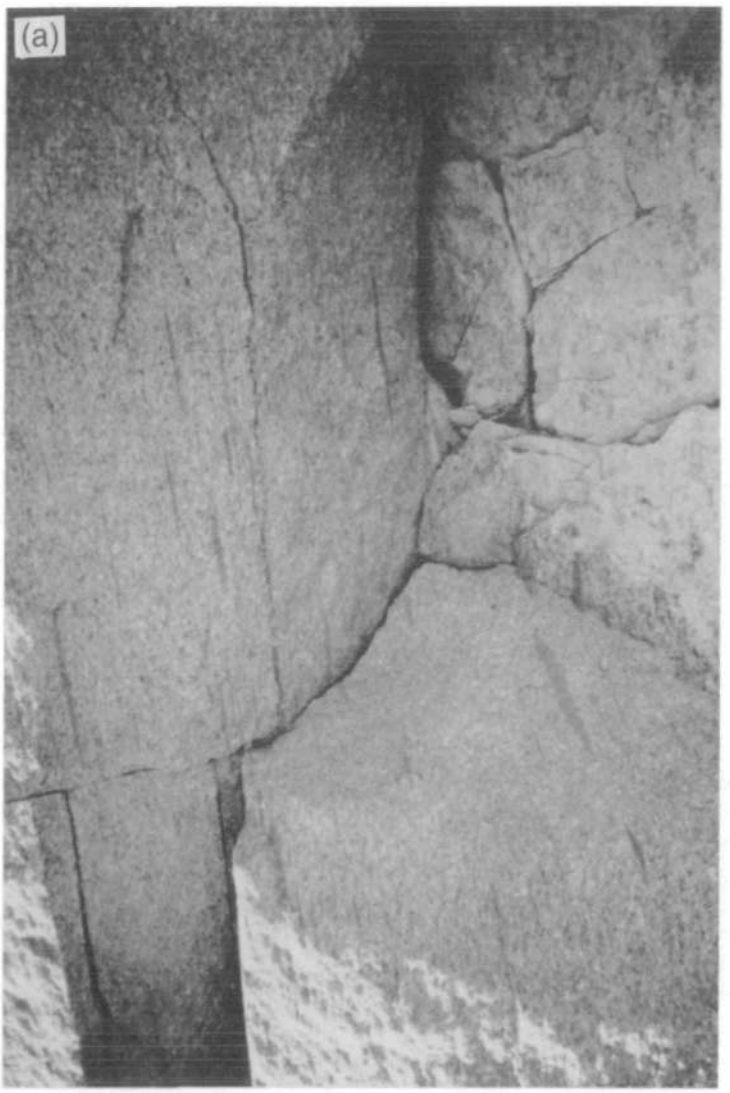

Fig. 7. (a) Foliation recorded by crystal and mafic enclave alignment in a granodiorite from the Sierra Nevada foothills (California, USA). The outcrop shows three orthogonal planes that facilitate the determination of the foliation trend. (b) Foliation recorded by K-feldspars in a biotite–muscovite-bearing granite, from the Fichtelgebirge massif (Germany). The notebook is oriented parallel to the foliation.

plutons (Pons *et al.*, 1995), in the Flamanville massif, in Brittany, France (Brun *et al.*, 1990), and in basic intrusions such as the Skaergaard Igneous Complex, Greenland (Nicolas, 1992). In the Saint Sylvestre massif, in the French Massif Central (Fig. 9), they are potential sites for major mineralization (Cuney *et al.*, 1990). These structures are interpreted as proto-plastic faults or magmatic shear zones (Blanchard, 1978; Mollier & Bouchez, 1982; Guineberteau *et al.*, 1987). Evidence for the high-temperature development of these structures is given by the plastic deformation of minerals (quartz, for example, in felsic rocks) over a certain width on each side of the proto-plastic fault. Conversely, K-feldspar veins may already show a brittle, or pseudo-brittle deformation (Fig. 8a).

Magma segregation under non-coaxial deformation differs from magma segregation by diffusion or by compaction as observed in basic magmas (Maaloe & Scheie, 1982; McKenzie, 1984; Shirley, 1987). In the case of filter pressing, gravity remains the main force, so the rate of extraction is limited by the permeability of the mush. Numerical values for low-viscosity tonalitic melts (10^4 Pa s) barely reach a compaction length of the order of a few hundred metres (Petford, 1993). Extraction rate is low and equilibrium is certainly achieved between the liquid and the residual solid. Conversely, because of the

Fig. 7. (b)

non-coaxial forces, rotational terms are introduced in the equations which lead to shear movements. This creates, locally, contractional areas from which melt is expelled and driven into dilatant sinks. The rate of magma movement is thus accelerated. As temperature falls, the diffusion time for elements is increased, and the segregated magma may not be at equilibrium.

As an example, we examine the Hercynian Saint Sylvestre granitic complex, French Massif Central (Fig. 9), in which important uranium deposits are located. Three major facies are recognized (Cuney *et al.*, 1990). The main facies (g_1) is a coarse-grained porphyritic granite which exhibits a dominant horizontal magmatic fabric. It outcrops over most of the complex, but its average thickness is small (2·6 km) as deduced from gravity data (Audrain *et al.*, 1989). Locally, fine-grained granites (facies g_2) are found as small intrusions in the facies g_1. Most of them (g_{2a}) occur as vertical sheets with vertical magmatic foliations trending north–south to N20, 0·5–1·5 km in width, and roughly conformable to facies g_1. In a few outcrops, fine-grained granites (g_{2b}) occur as thin sheets (of 50 m width), in sharp contact with g_1 and generally associated with shear zones, which display weakly dipping foliations and banding. The facies g_3 represents the most evolved type of granite. It displays sharp contacts with the other facies. g_2 and g_3 correspond to the more deeply rooted zones on the detailed gravity data (Fig. 9).

The genesis of the three main facies can be inferred from major and trace element studies (Cuney *et al.*, 1990). The granitic complex is part of an enriched portion of the Hercynian crust on the basis of heat flow and content of heat-producing elements (Vigneresse *et al.*, 1989). It has higher than normal U (10 p.p.m.) and Th (40 p.p.m.) contents, but these elements are still in the usual proportions relative to average granite values (Th/U = 4). The g_1 facies displays a fractionation trend common for granites (Fig. 10). As U increases, Th decreases because these elements have respectively an incompatible and compatible behaviour in low-temperature peraluminous melts. In the concordant g_{2a} facies, melt is extracted from the matrix, leading to Th-rich melts in which Th is concentrated in highly refractory minerals such as zircon and monazite. In the g_{2b} facies, corresponding to the most fractionated g_2 granites injected into weakly dipping magmatic shear zones, U increases with Th, but with a Th/U ratio near three. Uraninite becomes the major uranium-bearing phase. Residual melt injections, rich in uraninite, of g_{2b} type are also observed in small shear zones (a few centimetres in scale) over several hundred metres all around the g_2 bodies. In the g_3 facies, the Th/U trend is negative, similar to

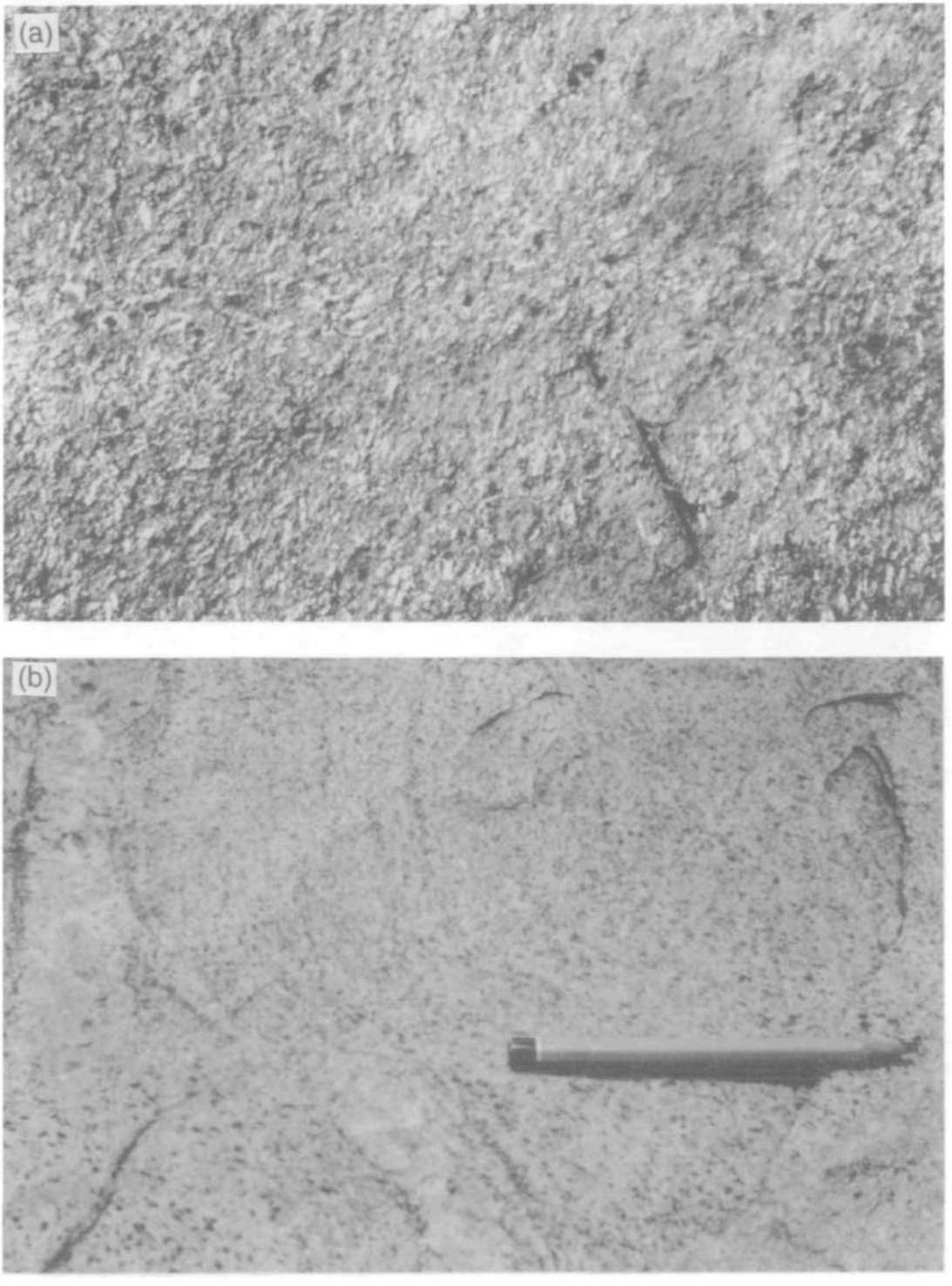

Fig. 8. (a) Protoplastic fault in the Mortagne granitic massif, in southern Brittany, reflected by the change of orientation of K-feldspars, which turn from a north–south trend toward a east–west trend in the centre of the photo. The size of the field is ~1 m. (b) Plastic deformation of a granitic magma, as shown by the curved foliation shown by the biotites, whereas the K-feldspar vein on the left is fractured, thus indicating that deformation occurred while magma was between 550 and 600°C, the temperature of brittle–ductile transition in feldspars.

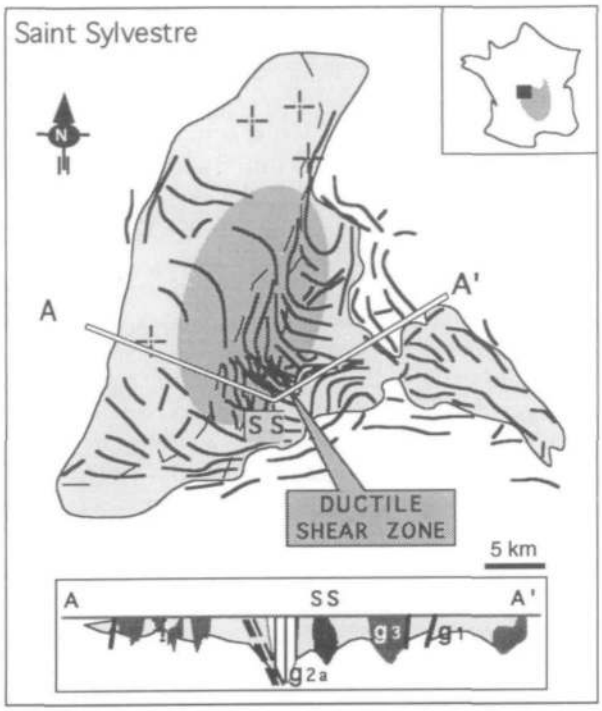

Fig. 9. Foliation map of the granitic massif of Saint Sylvestre (French Massif Central) redrawn from Mollier & Bouchez (1982). Emphasis is put on the magmatic, or proto-plastic, shear zone (within the ellipsoidal area in grey) which rotates the foliation planes in the centre of the massif. A cross-section of the massif is also drawn, based on the inversion of gravity data [after Audrain *et al.* (1989)], which shows the facies (g_{2a} and g_3) intrusive within the main facies g_1.

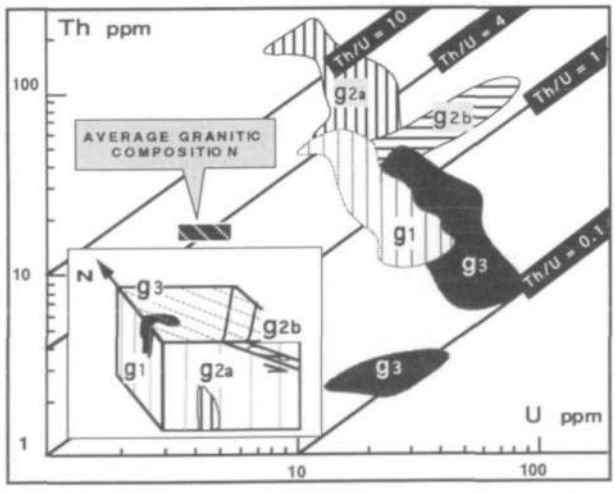

Fig. 10. Th–U diagram for granitoids from the Saint Sylvestre massif. The main facies g_1 shows a normal inverse correlation betwen Th and U. The two facies g_2 show opposite trends depending on whether they are concordant (g_{2a}) relative to g_1 (see inset) or discordant and associated with shear zones (g_{2b}). The late facies g_3 shows a normal Th–U fractionation trend, similar to g_1. Thus, according to the interaction between late deformation and chemical evolution of the magma, different trends are observed in the Th–U diagram, which reflect the late segregation of magma.

the g_{2a} pattern, but in this case, the increasing U content indicates that U is concentrated in uraninite. The observed shear zones are developed in the magmatic stage in g_2, whereas they form at a brittle stage in the g_3 facies. This therefore explains why the vicinity of g_2 and g_3 facies is the major potential site for U mineralization (Cuney *et al.*, 1990).

A similar change in the chemistry of the residual liquid can also be observed in the zonation of plagioclases, which changes from the borders of the massif towards its core (Loomis & Weber, 1982). When the system becomes totally locked, complete crystallization is achieved with no major changes to magma evolution and segregation. The only possibility left for magma to deform is through C-S structures (Gapais, 1989), yielding mylonites.

EFFECTS OF THE GEOMETRY OF PARTICLES

The distribution of the size and shape of coexisting particles induces poorly known effects on the general behaviour of crystal suspensions. During crystallization of crustally derived magma, minerals such as K-feldspar, plagioclase, biotite, amphibole and quartz have a tabular shape with an aspect ratio (long/short axis) ranging from 1 to 3. This ratio controls the rate at which particles rotate (Fernandez *et al.*, 1983). The shape of particles has important effects on the fabric the magma acquires when it starts to crystallize, and implications in determining the threshold melt percentage, especially for LPT and RPT, both depending on particle shape.

Effects on the fabrics

During magma emplacement, the flow remains mostly laminar, as indicated by the alignment of particles. For isolated particles, the shear strain γ_0 necessary for a particle of axial ratio n to achieve a complete rotation (Fernandez *et al.*, 1983) is

$$\gamma_0 = 4\pi/(1-k^2)^{1/2} \text{ with } k = (n^2-1)/(n^2+1) \quad (6)$$

thus resulting in

$$\gamma_0 = 2\pi(n+n^{-1}). \quad (7)$$

The increase of shear strain with the axial ratio n of particles approaches linearity because n is usually $>1{\cdot}0$ and $<3{\cdot}0$. Therefore, small elongated particles start to rotate before larger equant ones. This is recorded in the angular differences observed between subfabrics in minerals, for example, biotites and K-feldspars (Fernandez *et al.* 1983). Nevertheless, such a difference is only noticeable at the high values of shear used in modelling. It seems not to be the case

in laminar flows as commonly observed in real magma flows, which, in turn, implies highly viscous magma flows.

Independent contributions on liquid crystals by Dlugogorski *et al.* (1994) show similar pattern formation. These workers have computed the equation of motion of a system of interacting elliptical particles. The particles are free to rotate, within the limits of their respective interactions. At intermediate shear rates, ellipsoids become aligned with the direction of flow and the global shear tensor progressively begins to be non-symmetric. At higher shear rates, this configuration breaks down and a transition appears at a concentration of ~65% of particles. This leads to a highly ordered structure exhibiting general orientation of particles in the direction of the vorticity axis. Such a fabric also occurs in the phase transition between nematic and smectic phases (i.e. ordered to highly oriented within layers) observed for liquid crystals above 67·5% of particles (Dlugogorski *et al.*, 1994). This is similar to what is observed in our natural case at an equivalent concentration of solids. Thus, whatever their shape, spherical or ellipsoidal, particles are aligned by shear flow at the onset of random loose packing and then pass through a transition into a stable compact structure.

Effects on the packing value

Particle geometry affects packing values. For spherical particles, the regular packing density is simply computed from the volume distribution of uniform spheres in a regular system (face-centred cubic or body-centred cubic). This ranges from 55 to 64%. Random packing of uniform spheres is a little more difficult. Numerical simulations provide a value of 74% for the maximum volume fraction of solid (ϕ_{max}) (Rogers *et al.*, 1994). The use of a polydisperse system of spherical particles is also realized by numerical simulations and depends on the respective abundance of each group of particles. The packing is never complete, as any packing of spheres can not fill adequately a rectangular volume. A virtual magma, developing cubic grains of similar size, could achieve a dense packing value of 100%, provided strain and cooling rate are slow enough to achieve the organization of particles in a cubic frame. In such a case, RPT remains unchanged at $\phi = 55\%$, but complete packing, or PLT, would never have been reached before complete crystallization of the magma. The adopted value of RPT corresponds to the strong increase in the viscosity observed during experimental picrite crystallization (Ryerson *et al.*, 1988). Our suggested value of 72–75% solids for PLT can be considered as the symmetric of the one of the MET (P= 20–25%), which marks the transition from a coherent to a loose system. It corresponds to an interconnected pore network through which melt is connected. A further step in our model could be introduced, according to Bryon *et al.* (1996), marking the end of connection between liquid pores, preventing late circulation of the liquid, and thus diffusion.

Mafic enclaves can be considered as clusters of particles, mineralogically individualized, embedded in a magma of different composition. When submitted to strain, both the interstitial melt in the surrounding magma and the liquid contained in the enclaves are squeezed out of the whole system. This process is similar to pressure-dissolution and hydraulic fracturing. It results in fractured adjoining enclaves (Bédard, 1993*a*, 1993*b*) of which the shape is indicative of the strain history they record (Williams & Tobisch, 1994). They represent a specific mode of melt segregation during magma emplacement.

EXTENSION OF THE MODEL TO NON-FELSIC MAGMAS

We have already stated that our model relates to felsic material, with application to migmatites and granites. Nevertheless, as the model relates to physical phenomena, it certainly also applies to other types of magma. We briefly examine to what extent the rheological transitions we propose for felsic magmas also apply to more mafic melts extracted from the mantle (Fig. 11), though mineralogy, strain and temperature are different.

Mantle and crustal materials strongly differ in their mineralogy, olivine representing by far the most abundant mineral in mantle rocks. Furthermore, its intrinsic anisotropy reinforces its shape preferred orientation (Nicolas, 1992), which is reflected in the anisotropy of melt distribution (Hirth & Kohldstedt, 1995; Jin *et al.*, 1995). Conversely, crustal material involves at least three major minerals (quartz, plagioclase and K-feldspar) without any preferential anisotropy under shear. Because of the anisotropic distribution of grains, melt connectivity is more easily realized in mantle materials and melt can be extracted at a much lower melt percentage. Connectivity and melt percentages as low as a few percent have been suggested from experimentally deformed olivines (Hirth & Kohldstedt, 1995; Jin *et al.*, 1995). However, the threshold value for mantle-derived magmas is certainly higher, but below 5%, owing to the influence of pyroxenes, which are less wettable compared with olivine

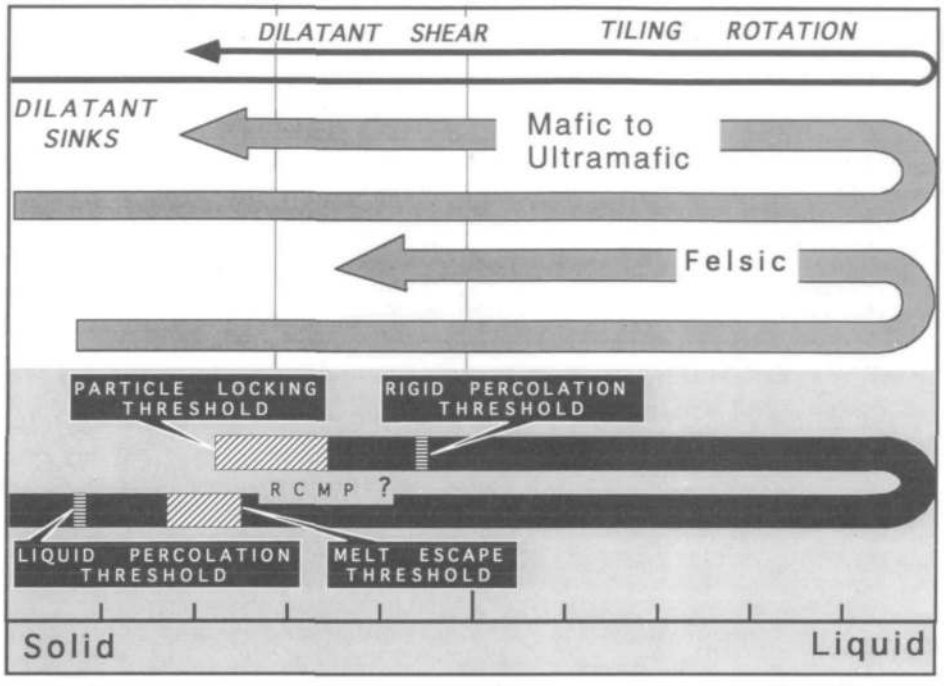

Fig. 11. Schematic representation of a complete magmatic cycle, from solid to liquid and then back to crystallization. At the onset of partial melting, magma goes through a percolation process and variable transition thresholds. Structural effects are represented in italics. When crystallizing, magma goes through a percolation and a transition threshold. Felsic magma paths are shorter than for mafic or ultramafic magmas derived from the mantle. Segregation operates earlier in the mantle but the melt and its matrix remain in equilibrium for a longer time. Late magma segregation of gabbros can operate up to 80% solid. Conversely, crustal derived magmas are more likely to be in disequilibrium and thus preserve more variable textures.

(Nakano & Fujii, 1989). Thus, the threshold value of melt connectivity (LPT) is reduced during partial melting of ultramafic rocks compared with felsic rocks.

The nature of the deformation and the strain rate at which mantle-derived magma segregates is certainly different from that of magma derived from the continental crust. Diapiric, or gravity-induced upwelling is strongly dependent on the rate at which the surrounding material can flow. Thus, the rheology of the matrix severely constrains the vertical movement of the magma. The bulk plastic behaviour of the upper mantle makes possible the segregation and transport of melt (plus its matrix) by diapiric upwelling over large distance and volume (Weinberg & Podladchikov, 1994), but even in this case, the compaction length remains small (McKenzie, 1984; Petford, 1993).

In the continental crust, vertical or gravity driven movement is restricted by the highly ductile lower crust, and prevented by the brittle nature of the upper crust (Vigneresse, 1995). Intimate association of non-coaxial deformation with crustal magmas (migmatites or granites) reflects the stronger resistance of the surrounding crust, which can sustain stress. The average stress level being higher, it increases the Mohr circle so that mode II fractures (shear) can develop if melt is present. In comparison, ductile and flowing mantle rocks present a lower resistance to stress, thus favouring mode I (extension) fractures through which melt is collected. The difference between crustal and mantle melt extraction reflects the predominance of gravity driven forces in the mantle versus non-coaxial deformation in the crust.

Crystallization of mantle-derived materials (e.g. peridotites in ophiolites) occurs at slowly varying deformation rate. Consequently, the magma flow pattern is regular over large distances compared with that observed in restricted felsic intrusions. Late-stage melt segregation is thus enhanced, whereas the expelled melt remains in contact with rocks in which the chemistry does not vary significantly. This restricts the variability of ultramafic facies. Because of the high temperature of crystallization and small strain rate, denser packing of mantle-derived magmas can be achieved by plastic deformation of grains, highly activated at these temperatures. This shifts the maximal close packing (RPT) to higher values, as high as 80% in ophiolite gabbros (Nicolas & Ildefonse, 1996). In consequence, the total length of the path followed by

initial melts up to late crystallization stages for mafic to ultramafic magmas starts before and ends after that of felsic magmas (Fig. 11). This longer time for melt–solid interactions favours achievement of equilibrium between melt and matrix, and thus reduces the possibility of having a large variety of facies of mantle-derived rocks.

The observation of a coherent fabric pattern with no return flow in granitic intrusions certainly precludes a vigorous convection in these magmas. In agreement with the absence of return flow, there is no significant chemical variation in vertical sections of eroded plutons, as shown for instance from trace element or heat-producing element (U, Th, K) distributions (Sawka & Chappell, 1988; Vigneresse & Cuney, 1991). This precludes compositional convection as systematically observed, for instance, in komatiites with an upper spinifex zone and lower olivine-rich layers (Arndt, 1986).

Equilibrium and disequilibrium textures

The association of melt and crystals implies chemical exchanges between both phases under changing physical conditions. Provided they are in contact for sufficient time, element exchange by diffusion is likely and equilibrium textures can be achieved. The time during which diffusion is possible depends upon the rate to which melt is extracted (Sawyer, 1994). Mantle-derived magmas are often in chemical equilibrium (Hoffman & Hart, 1978) because of the low extraction rate and activated diffusion under high-temperature conditions. In crustal magmas, produced at high temperature under granulite-facies conditions in the lower crust, diffusivity is activated whereas plastic deformation accommodates movements at a lower strain rate. The rates at which melt is produced and segregates are of the same order of magnitude, which generally results in equilibrium textures (Reid, 1990). In migmatites, the temperature at which exchange is likely to occur is relatively low (650–750°C), and does not stimulate diffusion. Melt equilibration is controlled by the slowest diffusing element. Values range from 6×10^{-11} m^2/s for K, 3×10^{-11} m^2/s for Na, to 3×10^{-12} m^2/s for Si, or Al, for granite–basalt interactions (Van der Laan & Wyllie, 1993) and can be as low as 10^{-20} m^2/s for trace elements such as Ce. However, non-coaxial deformation leads to fast, up to catastrophic, strain (10^{-2}–10^{-4} s^{-1}), compared with the compaction rate under gravity forces, which depends on matrix relaxation (10^{-10}–10^{-12} s^{-1}) if Nabarro–Herring creep is considered. Consequently, melts in migmatites, which are extracted at a fast rate and at relatively low melt percentage, are likely to show disequilibrium textures, and non-equilibrium chemical compositions (Barbey *et al.*, 1990; Sawyer, 1991). When the degree of melting is higher, but associated with a low extraction rate, then felsic melts have time to equilibrate.

Therefore, the probability of having textural or chemical equilibrium is lower in crustal-derived magmas than in mantle-derived magmas, because of the higher extraction rate and often enhanced diffusion owing to lower temperatures of crustal magmas

CONCLUSIONS

We suggest that the transitions from solid to liquid (partial melting) and liquid to solid (crystallization) are two separate processes which are not symmetrical with respect to each other. Consequently, one unique threshold, as proposed in Arzi's (1978) rheological critical melt percentage (RCMP) should not be used. Instead, we propose two thresholds for each transition. One, liquid percolation threshold (LPT) and rigid percolation threshold (RPT), respectively, is defined according to percolation theory whereas the other, melt escape threshold (MET) and particle locking threshold (PLT), respectively, varies according to deformation and particle shape. Neither transition is simply the converse of the other. In the case of melting, pockets of melt have to be connected to afford a path to the escaping magma. This is a bond-percolation, in the sense of the physical percolation theory. In the case of crystallization, randomly distributed solid particles mechanically interact, and contacts between them can propagate forces, resulting in a site-percolation. Consequently, thresholds are lower for partial melting compared with those for crystallization.

The suggested values we propose apply to felsic melts. They differ for mafic or ultramafic magmas, though the mechanisms remain similar. In addition, the main forces which control melt segregation and movement are gravity driven forces for mantle-derived magmas and non-coaxial deformation for crustal melts.

ACKNOWLEDGEMENTS

This paper started from fruitful discussions between structural geologists, geophysicists and petrologists. We must admit that the finding of a common scale of observation and language has not been so easy. We overcame this problem after many discussions with, among others, J. L. Bouchez, T. Rushmer, B. Ildefonse and H. Stunitz, who encouraged us to improve the manuscript once problems were identified and the consequent literature was discerned. Ed. Sawyer

and Marge Wilson are thanked for their efforts in editing the manuscript. Dan McKenzie suggested the problem of textural equilibrium for granites compared with granulites and ultramafic rocks. We also acknowledge E. Jardim de Sa, who kindly guided one of us (J.L.V.) to the Currais Novos migmatites and Paraiba gneisses in NE Brazil, and M. Brouand who shared his experience and photographs of Himalayan migmatites. P. Lagrange (CREGU) provided his time and his skill in improving the design of illustrations.

REFERENCES

Arndt, N., 1986. Differentiation in komatiites flows. *Journal of Petrology* **27**, 279–301.

Arzi, A. A., 1978. Critical phenomena in the rheology of partially melted rocks. *Tectonophysics* **44**, 173–184.

Audrain, J., Vigneresse, J. L., Cuney, M. & Friedrich, M., 1989. Modèle gravimétrique et mise en place du complexe granitique hyperalumineux de Saint-Sylvestre–Saint Goussaud (Massif Central français). *Comptes Rendus Hebdomadaires des Séances de l'Académie des Sciences* **309**(2), 1907–1914.

Babic, M., 1993. On the stability of rapid granular flows. *Journal of Fluid Mechanics* **254**, 127–150.

Babic, M., Shen, H. M. & Shen, H. T., 1990. The stress tensor in granular shear flows of uniform, deformable disks at high solids concentration. *Journal of Fluid Mechanics* **219**, 81–118.

Bagnold, R. A., 1954. Experiments on a gravity-free dispersion of large solid spheres in a Newtonian fluid under shear. *Proceedings of the Royal Society of London*, Series **A 225**, 49–53.

Barbey, P., Allé, P., Brouand, M. & Albarède, F., 1995. Rare-earth patterns in zircons from the Manaslu granite and Tibetan slab migmatites (Himalaya): insights in the origin and evolution of a crustally-derived granite magma. *Chemical Geology*, **125**: 1–17.

Barbey, P., Macaudière, J. & Nzenti, J. P., 1990. High-pressure dehydration melting of metapelites. Evidence from the migmatites of Yaoundé (Cameroon). *Journal of Petrology* **31**, 401–427.

Barnes, H. A., 1989. Shear-thickening ('Dilatancy') in suspensions on non-aggregating solid particles dispersed in Newtonian liquids. *Journal of Rheology* **33**, 329–366.

Barrière, M., 1976. Flowage differentiation: limitation of the 'Bagnold effect' to the narrow intrusions. *Contributions to Mineralogy and Petrology* **55**, 139–145.

Bashir, Y. M. & Goddard, J. D., 1991. A novel simulation method for the quasi-static mechanics of granular assemblages. *Journal of Rheology* **35**, 849–885.

Batchelor, G. K., 1976. Brownian diffusion of particles with hydrodynamic interaction. *Journal of Fluid Mechanics* **75**, 1–25.

Batchelor, G. K., 1983. Diffusion in a dilute polydisperse system of interacting spheres. *Journal of Fluid Mechanics* **131**, 155–175.

Baxter, G. W. & Behringer, R. P., 1991. Cellular automata models for the flow of granular materials. *Physica* **D51**, 465–471.

Bédard, L. P., 1993*a*. Injections multiples de magmas dans un conduit nourricier: implications sur le remplissage des plutons et l'extraction des magmas. *Canadian Journal of Earth Sciences* **30**, 124–131.

Bédard, L. P., 1993*b*. Significance of enclaves' roundness: an inherent characteristic? *Journal of Geology* **101**, 121–125.

Bergantz, G., 1992. Conjugate solidification and melting in multicomponent open and closed systems. *International Journal of Heat and Mass Transfer* **35**, 533–543.

Blanchard, J. P., 1978. Dynamique magmatique du granite porphyroïde des Ballons (Vosges méridionales). 'Fluidalité planaire' et 'couloirs magmatiques'. Phénomènes de percolation. *Bulletin de la Société géologique de France* **20**, 157–162.

Blanchard, J. P., Boyer, P. & Gagny, C., 1979. Un nouveau critère de sens de mise en place dans une caisse filonienne: le pincement aux épontes. *Tectonophysics* **53**, 1–25.

Blumenfeld, P., 1983. Le 'tuilage des mégacristaux', un critère d'écoulement rotationnel pour les fluidalités des roches magmatiques: application au granite de Barbey-Seyroux (Vosges). *Bulletin de la Société géologique de France* **25**, 309–318.

Blumenfeld, P. & Bouchez, J. L., 1988. Shear criteria in granite and migmatite deformed in the magmatic and solid states. *Journal of Structural Geology* **10**, 361–372.

Brouand, M., Blanzet, G. D. & Barbey, P., 1990. Zircon behaviour during crustal anatexis. Evidence from the Tibetan slab migmatites (Nepal). *Journal of Volcanology and Geothermal Research* **44**, 143–161.

Brown, M., Averkin, Y. A., McLellan, E. L. & Sawyer, E., 1995. Melt segregation in migmatites. *Journal of Geophysical Research* **100**, 15655–15679.

Brun, J. P. & Martin, H., 1978. Relations métamorphisme–déformation au cours de l'évolution dynamique d'un dôme migmatitique: le massif de Saint Malo (France). *Bulletin de la Société géologique de France* **20**, 91–101.

Brun, J. P., Gapais, D., Cogné, J. P., Ledru, P. & Vigneresse, J. L., 1990. The Flamanville granite (NW France): an unequivocal example of an expanding pluton. *Geological Journal* **25**, 271–286.

Bryon, D. N., Atherton, M. P., Cheadle, M. J. & Hunter, R. H., 1996. Melt movement and the occlusion of porosity in crystallizing granitic systems. *Mineralogical Magazine* **60**, 163–170.

Burg, J. P. & Vanderhaeghe, O., 1993. Structures and way-up criteria in migmatites, with application to the Velay dome (French Massif Central). *Journal of Structural Geology* **15**, 1293–1301.

Campbell, C. S., 1990. Rapid granular flows. *Annual Review of Fluid Mechanics* **22**, 57–92.

Carter, W. C., 1988. The forces and behavior of fluids constrained by solids. *Acta Metallurgica* **38**, 2283–2292.

Cazabat, A. M., 1991. Wetting films. *Advances in Colloid and Interface Science* **34**, 73–88.

Chvoj, Z., 1993. Kinetics of the non-equilibrium phase transformations. *Journal of Non-equilibrium Thermodynamics* **18**, 201–265.

Clemens, J. D. & Vielzeuf, D., 1987. Constraints on melting and magma production in the crust. *Earth and Planetary Science Letters* **86**, 287–306.

Cooper, R. F., 1990. Differential stress-induced melt migration: an experimental approach. *Journal of Geophysical Research* **95**, 6979–6992.

Coussot, P., 1994. Steady, laminar flow of concentrated mud suspensions in open channels. *Journal of Hydraulic Research* **32**, 535–559.

Cox, R. G. & Brenner, H., 1971. The rheology of a suspension of particles in a Newtonian fluid. *Chemical Engineering Science* **26**, 65–93.

Cuney, M. & Barbey, P., 1981. Mise en évidence de phénomènes de cristallisation fractionnée dans les migmatites. *Comptes Rendus Hebdomdaires des Séances de l'Académie des Sciences* **295**(2), 37–42.

Cuney, M., Friedrich, M., Blumenfeld, P., Bourguignon, A., Boiron, M. C., Vigneresse, J. L. & Poty, B., 1990. Metallogenesis in the French part of the Variscan orogen. Part I: U preconcentrations in the pre-Variscan formations: a comparison with Sn, W and Au. *Tectonophysics* **177**, 39–57.

Daines, M. J. & Richter, F. M., 1988. An experimental method for directly determining the interconnectivity of melt in a partially molten system. *Geophysical Research Letters* **15**, 1459–1462.

Davidson, C., Schmid, S. M. & Hollister, L. S., 1994. Role of melt during deformation in the deep crust. *Terra Nova* **6**, 133–142.

De Gennes, P. G., 1979. Conjectures on the transition from Poiseuille to plug flow in suspensions. *Journal de Physique* **40**, 783–787.

Dell'Angelo, L. N. & Tullis, J., 1988. Experimental deformation of partially melted granitic aggregates. *Journal of Metamorphic Geology* **6**, 495–615.

Dlugogorski, B. Z., Grmela, M., Carreau, P. J. & Lebon, G., 1994. Rheology of several hundred bodies. *Journal of Non-Newtonian Fluid Mechanics* **53**, 25–64.

Drake, T. G., 1990. Structures features in granular flows. *Journal of Geophysical Research* **95**, 8681–8696.

Einstein, A., 1906. Eine neue Bestimmung der Molekuldimensionnen. *Annales de Physique* **19**, 289–306.

Ernst, R. E. & Baragar, W. R. A., 1992. Evidence from magnetic fabric for the flow pattern of magma in the Mackenzie giant radiating dyke swarm. *Nature* **356**, 511–513.

Fernandez, A., 1987. Preferred orientation developed by rigid markers in two dimensional simple shear strain: a theoretical and experimental study. *Tectonophysics* **136**, 151–158.

Fernandez, A., Feybesse, J. L. & Mezure, J. F., 1983. Theoretical and experimental study of fabric developed by different shaped markers in two-dimensional simple shear. *Bulletin de la Société géologique de France* **25**, 319–326.

Fourcade, S., Martin, H. & d'Ars, J. de Bremond, 1992. Chemical exchange in migmatites during cooling. *Lithos* **28**, 43–53.

Fowler, A. C., 1987. Theories of mushy zones: applications to alloy solidification, magma transport, frost heave and igneous intrusions. In: Loper, D. E. (ed.) *Structure and Dynamics of Partially Solidified Systems*, Nato ASI Series E125. Dordrecht: Martinus Nijhoff, pp. 159–199.

Gapais, D., 1989. Shear structures within deformed granites: mechanical and thermal indicators. *Geology* **17**, 1144–1147.

Gapais, D. & Barbarin, B., 1986. Quartz fabrics transition during cooling of syntectonic granite (Hermitage massif, France). *Tectonophysics* **125**, 357–370.

Garboczy, E. J. & Thorpe, M. F., 1985. Effective medium theory of percolation on central force elastic networks. II Further results. *Physical Review* **B31**, 7276–7280.

Gleizes, G., Nedelec, A., Bouchez, J. L., Autran, A. & Rochette, P., 1993. Magnetic susceptibility of the Mont Louis, Andorra, ilmenite type granite (Pyrenees): a new tool for the petrographic characterization and regional mapping of zoned granite plutons. *Journal of Geophysical Research* **98**, 4317–4331.

Grinfeld, M. A., 1993. The stress driven instability in elastic crystals: mathematical models and physical manifestations. *Journal of Non-linear Science* **3**, 35–83.

Guineberteau, B., Bouchez, J. L. & Vigneresse, J. L., 1987. The Mortagne granite pluton (France) emplaced by pull apart along a shear zone: structural and gravimetric arguments, regional implication. *Geological Society of America Bulletin* **99**, 763–770.

Guyon, E., Roux, S., Hansen, A., Bideau, D., Troadec, J. P. & Crapo, H., 1990. Non-local and non-linear problems in the mechanics of disordered systems: application to granular media and rigidity problems. *Report on Progress in Physics* **53**, 373–419.

Hand, M. & Dirks, P. H. G. M., 1992. The influence of deformation of axial planar leucosomes and the segregation of small melt bodies within the migmatitic Napperby gneiss, Central Australia. *Journal of Structural Geology* **14**, 591–604.

Harren, S. V., Dève, H. E. & Asaro, R. J., 1988. Shear band formation in plane strain compression. *Acta Metallurgica* **38**, 2435–2480.

Hibbard, M. J. & Watters, R. S., 1985. Fracturing and diking in incompletely crystallized granitic plutons. *Lithos* **18**, 1–12.

Hirth, G. & Kohlstedt, D. L., 1995. Experimental constraints on the dynamics of the partially molten upper mantle: deformation in the diffusion creep regime. *Journal of Geophysical Research* **100**, 1981–2001.

Hoffman, A. W. & Hart, S. R., 1978. An assessment of local and regional equilibrium in the mantle. *Earth and Planetary Science Letters* **38**, 44–62.

Holtz, F. & Johannes, W., 1994. Maximum and minimum water contents of granitic melts, implications for chemical and physical properties of ascending magmas. *Lithos* **32**, 149–159.

Hori, M. & Yonezawa, F., 1975. Statistical theory of effective electrical, thermal, and magnetic properties of random heterogeneous materials. IV. Effective-medium theory and cumulant expansion method. *Journal of Mathematical Physics* **16**, 352–364.

Hutter, K. & Koch, T., 1991. Motion of a granular avalanche in an exponentially curved chute: experiments and theoretical predictions. *Proceedings of the Royal Society of London, Series* **A 334**, 93–138.

Ildefonse, B., Launeau, P., Bouchez, J. L. & Fernandez, A., 1992. Effect of mechanical interactions on the development of shape preferred orientations: a two dimensional experimental approach. *Journal of Structural Geology* **14**, 73–83.

Jenkins, J. T. & Savage, S. B., 1983. A theory for the rapid flow of identical smooth, nearly elastic particles. *Journal of Fluid Mechanics* **130**, 187–202.

Jin, Z. M., Green, H. W. & Zhou, Y., 1995. Melt topology in partially molten mantle peridotite during deformation. *Nature* **372**, 164–167.

Jinescu, V. V., 1974. The rheology of suspensions. *International Chemical Engineering* **14**, 397–420.

Johannes, W., 1988. What controls partial melting in migmatites? *Journal of Metamorphic Geology* **6**, 451–465.

John, B. E. & Stunitz, H., 1997. Evidence for magma fracturation and small scale melt segregation during pluton emplacement. In: Bouchez, J. L., Hutton, D. H. & Stephens E. S. (eds) *Granites: from Segregation of Melt to Emplacement Fabric*. Dordrecht: Kluwer Academic 55–75.

Jones, K. A. & Brown, M., 1990. High-temperature 'clockwise' *P–T* paths and melting in the development of regional migmatites: an example from southern Brittany, France. *Journal of Metamorphic Geology* **8**, 551–578.

Jurewicz, S. R. & Watson, E. B., 1985. The distribution of partial melt in a granitic system: the application of liquid phase sintering theory. *Geochimica et Cosmochimica Acta* **49**, 1109–1121.

Komar, P. D., 1976. Phenocryst interactions and the velocity profile of magma flowing through dikes or sills. *Geological Society of America Bulletin* **87**, 1336–1342.

Kröner, E., 1978. Self-consistent scheme and graded disorder in polycrystal elasticity. *Journal of Physics* **F8**, 2261–2267.

Laporte, D., 1994. Wetting behavior of partial melts during crustal anatexis: the distribution of hydrous silicic melts in poly-

crystalline aggregates of quartz. *Contributions to Mineralogy and Petrology* **116**, 486–499.

Laporte, D. & Watson, E. B., 1995. Experimental and theoretical constraints on melt distribution in crustal sources: the effect of crystalline anisotropy on melt interconnectivity. *Chemical Geology* **124**, 161–184.

Lejeune, A. M. & Richet, P., 1995. Rheology of crystal-bearing silicate melts: an experimental study of high viscosities. *Journal of Geophysical Research* **100**, 4215–4229.

Loomis, T. P. & Weber, P. W., 1982. Crystallization processes in the Rocky Hill granodiorite pluton, California: an interpretation based on compositional zoning of plagioclase. *Contributions to Mineralogy and Petrology* **81**, 230–239.

Maaloe, S., 1992. Melting and diffusion processes in closed-system migmatization. *Journal of Metamorphic Geology* **10**, 503–516.

Maaloe, S. & Scheie, A., 1982. The permeability controlled accumulation of primary magma in a planetary mantle. *Physics of the Earth and Planetary Interiors* **29**, 344–353.

Macaudière, J., Barbey, P., Jobbari, J. & Marignac, C., 1992. Le stade initial de fusion dans le dévelopement des dômes anatectiques: le dôme du Velay (Massif Central français). *Comptes Rendus Hebdomadaires des Séances de l'Académie des Sciences* **315**(2), 1761–1767.

Major, J. J. & Pierson, T. C., 1992. Debris flow rheology: experimental analysis of fine-grained slurries. *Water Resources Research* **28**, 841–857.

Marsh, B. D., 1989. Magma chambers. *Annual Review of Earth and Planetary Sciences* **17**, 439–474.

McKenzie, D., 1984. The generation and compaction of partially molten rocks. *Journal of Petrology* **25**, 713–765.

McLellan, E. L., 1988. Migmatite structures in the Central Gneiss Complex, Boca de Quadra, Alaska. *Journal of Metamorphic Geology* **6**, 517–542.

Mehnert, K. R. & Büsch, W., 1982. The initial stage of migmatite formation. *Neues Jahrbuch für Mineralogie, Abhandlungen* **145**, 211–238.

Miller, C. F., Watson, E. B. & Harrison, T. M., 1988. Perspectives on the source, segregation and transport of granitoid magmas. *Transactions of the Royal Society of Edinburgh* **79**, 135–156.

Mollier, B. & Bouchez, J. L., 1982. Structuration magmatique du complexe granitique de Brame–St Sylvestre–St Goussaud (Limousin, Massif Central français). *Comptes Rendus Hebdomadaires des Séances de l'Académie des Sciences* **294**(2), 1329–1333.

Montel, J. M., Marignac, C., Barbey, P. & Pichavant, M., 1992. Thermobarometry and granite genesis: the Hercynian low-P high-T Velay anatectic dome (French Massif Central). *Journal of Metamorphic Geology* **10**, 1–15.

Nakano, T. & Fujii, N., 1989. The multiphase grain control percolation: its implication for a partially molten rock. *Journal of Geophysical Research* **94**, 15653–15661.

Nicolas, A., 1986. A melt extraction model based on structural studies in mantle peridotites. *Journal of Petrology* **27**, 999–1022.

Nicolas, A., 1992. Kinematics in magmatic rocks with special reference to gabbros. *Journal of Petrology* **33**, 891–915.

Nicolas, A. & Ildefonse, B., 1996. Flow mechanism and viscosity in basaltic magma chambers. *Geophysical Research Letters* **23**, 2013–2016.

Nolan, G. T. & Kavanagh, P. E., 1992. Computer simulation of random packing of hard spheres. *Powder Technology* **72**, 149–155.

Nzenti, J. P., Barbey, P., Macaudière, J. & Soba, D., 1988. Origin and evolution of the late Precambrian high grade Yaoundé gneisses (Cameroon). *Precambrian Research* **38**, 91–109.

Ogawa, A., Cox, R. G. & Mason, S. G., 1973. The kinetics of flowing dispersion. VI Transect orientation and rheological properties of rods and discs in shear flow. *Journal of Colloid and Interface Science* **45**, 303–329.

Olsen, S. N., 1985. A quantitative approach to local mass balance in migmatites. In: Atherton, M. P. & Gribble, C. D. (eds) *Migmatites, Melting and Metamorphism*. Nantwich, UK: Shiva, pp. 201–233.

Onoda, G. Y. & Liniger, E. G., 1990. Random loose packing of uniform spheres and the dilatancy onset. *Physical Review Letters* **64**, 2727–2730.

Patiño Douce A. E. & Beard, J. S., 1995. Dehydration melting of biotite gneiss and quartz amphibolite from 3 to 15 kbar. *Journal of Petrology* **96**, 707–738.

Petford, N., 1993. Porous media flow in granitoid magmas: an assessment. In: Stone, D. B. & Runcorn, S. K. (eds) *Flow and Creep in the Solar System: Observations, Modeling and Theory*. Dordrecht: Kluwer Academic, pp. 261–286.

Pons, J., Barbey, P., Dupuis, D. & Léger, J. M., 1995. Mechanism of pluton emplacement and structural evolution of a 2·1 Ga juvenile continental crust: the Birimian of southwestern Niger. *Precambrian Research* **70**, 281–301.

Reid, M. R., 1990. Ionprobe investigation of rare earth element distributions and partial melting of metasedimentary granulites. In: Vielzeuf, D. & Vidal, P. (eds) *Granulites and Crustal Evolution*. Dordrecht: Kluwer Academic, pp. 507–522.

Ribe, N. M., 1987. Theory of melt segregation—a review. *Journal of Volcanology and Geothermal Research* **33**, 241–253.

Rogers, C. D. F., Dijkstra, T. A. & Smalley, T. A., 1994. Particle packing from an Earthscience viewpoint. *Earth-Science Reviews* **36**, 59–82.

Roscoe, R., 1952. The viscosity of suspensions of rigid spheres. *British Journal of Applied Physics* **3**, 267–269.

Rushmer, T., 1995. An experimental deformation study of partially molten amphibolite. Application to low fraction melt segregation. *Journal of Geophysical Research* **100**, 15681–15695.

Rutter, E. H. & Neumann, D. H. K., 1995. Experimental deformation of partially molten Westerly granite under fluid-absent conditions with implications for the extraction of granitic magma. *Journal of Geophysical Research* **100**, 15697–15715.

Ryerson, F. J., Weed, H. C. & Piwinskii, A. J., 1988. Rheology of subliquidus magmas. I. Picritic compositions. *Journal of Geophysical Research* **93**, 3421–3432.

Savage, S. B. & Sayed, M., 1984. Stresses developed by dry cohesionless granular materials sheared in annular shear cell. *Journal of Fluid Mechanics* **142**, 391–430.

Sawka, W. N. & Chappell, B. W., 1988. Fractionation of uranium, thorium and rare earth elements in a vertically zoned granodiorite: implications for the heat production distribution in the Sierra Nevada batholith, California, USA. *Geochimica et Cosmochimica Acta* **52**, 1131–1143.

Sawyer, E. W., 1991. Disequilibrium melting and the rate of melt residuum separation of mafic rocks from the Grenville Front, Québec. *Journal of Petrology* **32**, 701–738.

Sawyer, E. W., 1994. Melt segregation in the continental crust. *Geology* **22**, 1019–1022.

Sawyer, E. W. & Barnes, S. J., 1988. Temporal and compositional differences between subsolidus and anatectic migmatite leucosomes from the Quetico metasedimentary belt, Canada. *Journal of Metamorphic Geology* **6**, 437–450.

Sawyer, E. W. & Robin, P. Y. F., 1986. The subsolidus segregation of layer-parallel quartz–feldspar veins in greenschist to

upper amphibolite facies metasediments. *Journal of Metamorphic Geology* **4**, 237–260.

Schaeffer, D. G., 1992. A mathematical model for localization in granular flow. *Proceedings of the Royal Society of London, Series A* **436**, 217–250.

Shirley, D. N., 1987. Differentiation and compaction in the Palisades Sill, New Jersey. *Journal of Petrology* **28**, 835–865.

Stauffer, D., 1985. *Introduction to Percolation Theory*. London: Taylor & Francis, 124 pp.

Van der Laan, S. R. & Wyllie, P. J., 1993. Experimental interaction of granitic and basaltic magmas and implications for mafic enclaves. *Journal of Petrology* **34**, 491–517.

Van der Molen, I. & Paterson, M. S., 1979. Experimental deformation of partially melted granite. *Contributions to Mineralogy and Petrology* **70**, 299–318.

Vielzeuf, D. & Holloway, J. R., 1988. Experimental determination of the fluid-absent melting relations in the pelitic system. Consequence for crustal differentiation. *Contributions to Mineralogy and Petrology* **98**, 257–276.

Vigneresse, J. L., 1995. Control of granite emplacement by regional deformation. *Tectonophysics* **249**, 173–186.

Vigneresse, J. L. & Cuney, M., 1991. Are granites representative of heat flow provinces? In: Cermak, V. & Rybach, L. (eds) *Exploration of the Deep Continental Crust*. Heidelberg: Springer Verlag, pp. 56–110.

Vigneresse, J. L., Cuney, M. & Barbey, P., 1991. Deformation assisted crustal melt segregation and transfer. *Geological Association of Canada–Mineralogical Association of Canada Abstract* **16**, A128.

Vigneresse, J. L., Cuney, M., Jolivet, J. & Bienfait, G., 1989. Selective heat producing element enrichment in a crustal segment of the mid-European Variscan chain. *Tectonophysics* **159**, 47–60.

Waff, H. S. & Faul, U. H., 1992. Effects of crystalline anisotropy on fluid distribution in ultramafic partial melts. *Journal of Geophysical Research* **97**, 9003–9014.

Weber, C. & Barbey, P., 1986. The role of water, mixing processes and metamorphic fabric in the genesis of the Baume migmatites (Ardèche, France). *Contributions to Mineralogy and Petrology* **92**, 481–491.

Weber, C., Barbey, P., Cuney, M. & Martin, H., 1985. Trace element behaviour during migmatization. Evidence for a complex melt–residuum–fluid interaction in the St Malo migmatite dome (France). *Contributions to Mineralogy and Petrology* **90**, 52–62.

Weinberg, R. F. & Podladchikov, Y., 1994. Diapiric ascent of magmas through power law crust and mantle. *Journal of Geophysical Research* **99**, 9543–9559.

Wickham, S. M., 1987. The segregation and emplacement of granitic magma. *Journal of the Geological Society of London* **144**, 281–297.

Wildenmuth, C. R. & Williams, M. C. 1985. A new interpretation of viscosity and yield stress in dense slurries: coal and other irregular particles. *Rheologica Acta* **24**, 75–91.

Williams, Q. & Tobisch, O. T., 1994. Microgranitic enclave shapes and magmatic strain histories: constraints from drop deformation theory. *Journal of Geophysical Research* **99**, 24359–24368.

Worster, M. G., 1992. Instabilities of the liquid and mushy regions during solidifications of alloys. *Journal of Fluid Mechanics* **237**, 649–669.

RECEIVED SEPTEMBER 26, 1995
REVISED TYPESCRIPT ACCEPTED JULY 29, 1996